



**HAL**  
open science

# Identification of fracture models based on phase field for crack propagation in heterogeneous lattices in a context of non-separated scales

Nhu Nguyen, J. Yvonnet, Julien Réthoré, Anh Binh Tran

## ► To cite this version:

Nhu Nguyen, J. Yvonnet, Julien Réthoré, Anh Binh Tran. Identification of fracture models based on phase field for crack propagation in heterogeneous lattices in a context of non-separated scales. Computational Mechanics, 2019, 63 (5), pp.1047-1068. 10.1007/s00466-018-1636-z . hal-02265335

**HAL Id: hal-02265335**

**<https://hal.science/hal-02265335>**

Submitted on 9 Aug 2019

**HAL** is a multi-disciplinary open access archive for the deposit and dissemination of scientific research documents, whether they are published or not. The documents may come from teaching and research institutions in France or abroad, or from public or private research centers.

L'archive ouverte pluridisciplinaire **HAL**, est destinée au dépôt et à la diffusion de documents scientifiques de niveau recherche, publiés ou non, émanant des établissements d'enseignement et de recherche français ou étrangers, des laboratoires publics ou privés.

# Identification of fracture models based on phase field for crack propagation in heterogeneous lattices in a context of non-separated scales

Nhu Nguyen\*, J. Yvonnet\*, J. Réthoré<sup>†</sup>,  
A.B. Tran<sup>+</sup>

Received: date / Accepted: date

**Abstract** The construction of a homogeneous medium equivalent to a heterogeneous one under quasi-brittle fracture is investigated in the case of non-separated scales. At the microscale, the phase field method to fracture is employed. At the scale of the homogeneous medium, another phase field model either isotropic or anisotropic, depending on the microscale crack length and on the underlying microstructure, is assumed. The coefficients of the unknown phase field model for the homogeneous model are identified through the mechanical response of a sample subjected to fracture whose microstructure is fully described and estimated numerically. We show that the identified models can reproduce both the mechanical force response as well as overall crack paths with good accuracy in other geometrical configurations than the one used to identify the homogeneous model. Several numerical examples, involving cracking in regular lattices of both hard particles and pores, are presented to show the potential of the technique.

**Keywords** Phase field method, damage, homogenization, crack propagation, quasi-brittle materials, lattice structures

## 1 Introduction

Most of civil engineering materials are heterogeneous and quasi-brittle. In such materials, the macro cracks originate from microcracks which initiate at the mi-

---

Nhu Nguyen, J. Yvonnet(✉)  
Laboratoire Modélisation et Simulation Multi Échelle  
MSME UMR 8208 CNRS, Université Paris-Est  
5 bd Descartes, 77454 Marne-la-Vallée, France  
E-mail: julien.yvonnet@univ-paris-est.fr

J. Réthoré  
Institut de Recherche en Génie Civil et Mécanique-GeM  
UMR CNRS 6183, École Centrale de Nantes  
1 rue de la Noë 44321, Nantes, France.

A.B Tran  
National University of Civil Engineering  
55 Giai Phong street, Ha Noi, Vietnam.

crosscale, due to local stress concentrations or at the interfaces. Studying the crack propagation in such media is of high importance to predict the durability of civil engineering structures or a large variety of quasi-brittle heterogeneous media, like e.g. ceramics-ceramics composites in aerospace industry or cementitious porous media. However, direct numerical simulations involving an explicit description of microcracks and all heterogeneities is so far not tractable neither efficient to study cracking in engineering applications. It is then highly important to construct homogenized models able to reproduce accurately the damage in the structure, and involving reasonable computational times.

Homogenization of damage behavior in heterogeneous media is a tough topic due to several issues: (a) the intrinsic nonlinearity of the problem; (b) the difficulty to define an RVE due to sharp localization [? ? ]; (c) the numerical lack of convergence and stability at the macroscale; (d) the definition of the characteristic length scale at both scales. A large amount of studies and numerical methods have been proposed in the literature, mostly relying on numerical approaches.

When considering damage of thin heterogeneous interphases, several methods relying on concurrent multilevel Finite Element (FE<sup>2</sup>) [? ] have been proposed [? ? ? ? ], where an RVE is defined to either define a priori or concurrently define a cohesive model at the macroscale.

Considering crack propagation in heterogeneous structures where the crack path is not known in advance, several techniques extending the FE<sup>2</sup> to discontinuous problems at the macroscale have been proposed (see e.g. [? ? ? ]. Coenen et al. [? ] introduced an extension of FE<sup>2</sup> where the macroscopic kinematics were enriched with discontinuities to model localization bands at the microscale. In [? ], the technique was modified using an XFEM approximation and by introducing modified boundary conditions to take into account the non-periodicity of the field in the case of a crossing localization band within the RVE. In [? ], Oliver et al. introduced a similar approach based on the Continuum Strong Discontinuity Approach (CSDA), and provided an extension embedding model reduction in [? ].

Apart from FE<sup>2</sup>-like methods, domain decompositions constitute another family of approaches to handle damage in heterogeneous structures. In [? ], a domain decomposition method including discontinuities modeled by XFEM was proposed with a global/local solving procedure based on the LATIN method [? ]. Other domain decomposition methods embedding discontinuities were proposed, like based on Usawa's algorithm [? ], and adaptive multigrid solvers for XFEM approximations [? ].

Most of the above methods involve either costly computations related to concurrent multilevel calculations, and domain decomposition methods still have difficulties regarding convergence when propagating cracks occur.

In [? ], a different approach has been proposed, where the effective toughness of the heterogeneous media was directly evaluated a priori (without concurrent computations). The phase field method [? ? ? ? ] was used at the microscale to calibrate the effective toughness, defined as the macroscopic energy release rate required at the boundary of a heterogeneous representative domain to propagate the crack over a macroscopic distance.

In the present work, we follow the work of [? ] by identifying the different parameters of a damage model at the macroscale, which can then be used without concurrent computations for the macroscale calculations. However, in contrast to the mentioned work, we directly identify all the different parameters of the model,

by fitting a typical mechanical test response under crack initiation and propagation in a structure where all heterogeneities are explicitly described. More specifically, the macroscopic damage model is based on the phase field method and its extensions to anisotropic crack propagation [? ? ? ], to handle the effects of preferential crack propagation in regular lattices. The phase field method has several appealing advantages as compared to other models to describe crack propagation at the macroscale: (a) it allows crack nucleation, propagation and merging of complex 2D or 3D multiple crack networks by using classical finite elements and without discontinuous enrichment; (b) it is convergent, mesh-independent and stable, due to its intrinsic damage-gradient-based nature; (c) it involves a small number of parameters to be identified; (d) it has been shown to be very predictive with respect to experiments on cementitious materials both regarding the mechanical response and the local crack patterns, even in complex microstructures [? ? ].

The layout of the paper is as follows. In section 2, the phase field method to fracture, which is employed for the heterogeneous medium, is reviewed. In section 3, the proposed fracture models for the homogeneous medium, including both isotropic and anisotropic phase field models, are described. The identification procedure is provided. Numerical examples involving heterogeneous media including regular lattices with both hard inclusions and pores are provided in section 4 to evaluate the accuracy of the constructed models.

## 2 Fracture model within homogeneous phases of the heterogeneous medium

In this work, the variational approach to fracture as proposed originally by Francfort, Marigo [? ] is employed. The method has been recast in a regularized form in [? ] by Bourdin et al. and is nowadays called phase field method by most of authors [? ? ]. While in its original form the method estimated the energy based on unknown sharp discontinuities, the regularized approach uses a continuous (called damage) field to describe the discontinuities thanks to a Mumford - Shah functional as proposed in [? ], which gratefully simplifies the minimization process with respect to both displacements and damage fields. The regularization process involves a parameter  $\ell$ , which defines an internal length variable. The obtained models are close to gradient-enhanced damage models [? ] but differ regarding the following differences: (a) a convergence to the variational principle embedding true discontinuities as the internal length tends to zero; (b) an algorithmic structure where the damage field is obtained by solving a global problem over the structure. A recent review of the phase field method can be found in [? ].

In the following, we describe the equations describing the model of fracture for each homogeneous phase of the fully heterogeneous medium, defined in an open domain  $\Omega \subset \mathbb{R}^D$ , where  $D$  denotes the space dimension. The corresponding boundary of  $\Omega$  is denoted by  $\partial\Omega$ , where  $\partial\Omega = \partial\Omega_u \cup \Omega_F$ ,  $\partial\Omega_u \cap \Omega_F = \emptyset$ , where traction forces  $\mathbf{F}^*$  are prescribed over the boundary  $\partial\Omega_F$  and displacements  $\mathbf{u}^*$  are prescribed over the boundary  $\partial\Omega_u$  (see Fig. 1).

The solid may contain cracks denoted collectively as  $\Gamma$ . The solid is heterogeneous, including several phases with different elastic and fracture properties. Within each phase, we assume that the fracture process is isotropic. The total energy of the system is defined, in the absence of body forces, as:

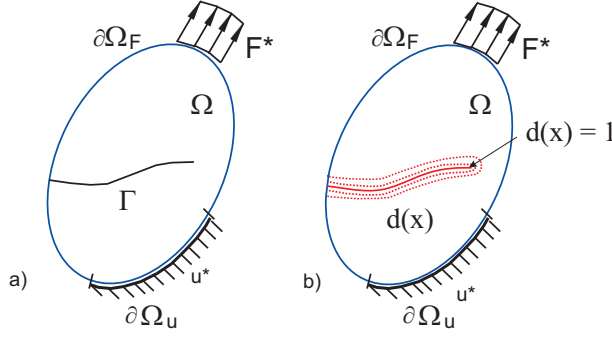


**Fig. 1:** (a) Sharp crack representation; (b) smeared crack representation in a solid domain.

$$E = \int_{\Omega} \Psi(\boldsymbol{\varepsilon}, \Gamma) d\Omega + g_c \int_{\Gamma} d\Gamma - \int_{\partial\Omega_F} \mathbf{F}^* \cdot \mathbf{u} d\Gamma \quad (1)$$

where  $\Psi(\boldsymbol{\varepsilon}, \Gamma)$  is the elastic strain density function and  $g_c$  is the critical energy release rate in the sense of Griffith. A regularized form is given by [? ? ]:

$$E = \int_{\Omega} \Psi(\boldsymbol{\varepsilon}, d) d\Omega + g_c \int_{\Omega} \gamma(d, \nabla d) d\Omega - \int_{\partial\Omega_F} \mathbf{F}^* \cdot \mathbf{u} d\Gamma, \quad (2)$$

where  $\gamma$  denotes the crack density function, and

$$\Psi = g(d)\Psi^+(\boldsymbol{\varepsilon}^+) + \Psi^-(\boldsymbol{\varepsilon}^-), \quad (3)$$

where  $g(d)$  is a degradation function such that  $g(0) = 1$ ,  $g(1) = 0$  and  $g'(1) = 0$  and  $\Psi^+(\boldsymbol{\varepsilon}^+)$  and  $\Psi^-(\boldsymbol{\varepsilon}^-)$  denote parts of the strain density related to tensile and compressive parts of the strain tensor, respectively (see [? ]), which are defined here by:

$$\Psi^{\pm}(\boldsymbol{\varepsilon}) = \lambda(\langle \text{Tr}(\boldsymbol{\varepsilon}) \rangle_{\pm})^2 / 2 + \mu \text{Tr}\{(\boldsymbol{\varepsilon}^{\pm})^2\}. \quad (4)$$

This form allows avoiding interpenetration when the cracks are closed without any special algorithm for auto-contact, which renders the implementation very simple. In (4),  $\lambda$  and  $\mu$  denote the elastic Lamé's constants in each phase. The operator  $\langle \cdot \rangle_{\pm}$  is defined as  $\langle x \rangle_{\pm} = (x \pm |x|) / 2$ ,  $\boldsymbol{\varepsilon}^+$  is the tensile part while  $\boldsymbol{\varepsilon}^-$  is the compression part of the strain tensor obtained by the spectral decomposition:

$$\boldsymbol{\varepsilon}_{\pm} = \sum_{i=1}^n \langle \text{Tr}(\boldsymbol{\varepsilon}) \rangle_{\pm} \mathbf{v}_i \otimes \mathbf{v}_i \quad (5)$$

in which  $\mathbf{v}_i$  are the eigenvectors of the strain tensor  $\boldsymbol{\varepsilon}$ . Other decompositions have been proposed as in [? ? ].

The variational approach to fracture as proposed in Bourdin, Francfort and Marigo [? ? ? ] and developed in a convenient algorithmic setting by Miehe [? ] is adopted here. The phase field formulation implies: (a) minimization of the total energy with respect to the displacement field  $\mathbf{u}$  and (b) minimization of the energy with respect to the scalar field  $d$  describing the crack surface in a smooth manner. This second minimization is subjected to an inequality constraint:  $\dot{d} \geq 0$ . To formulate this minimization problem in a simpler setting, a time-stepping

$\mathcal{T} = \{t^0, t^1, \dots, t^n, t^{n+1}, \dots, t^N\}$  is introduced. At each time step  $t^{n+1}$ , the problem is to find the displacement fields  $\mathbf{u}^{n+1}$  and  $d^{n+1}$  such that

$$\mathbf{u}^{n+1}, d^{n+1} = \underset{\substack{\mathbf{u} \in \mathcal{K}_A \\ 0 \leq d^n \leq d^{n+1}}}{\text{Arg min}} E \quad (6)$$

where  $\mathcal{K}_A$  is a set of kinematically admissible fields. One possible algorithm (adopted in the present work) to solve this problem is to use sequential solving of both minimization problems as

$$D_{\delta \mathbf{u}} \mathcal{L} = 0 \quad (7)$$

$$D_{\delta d} \mathcal{L} = 0, \quad 0 \leq d^n \leq d^{n+1}. \quad (8)$$

where  $D_{\delta \mathbf{v}} f(\mathbf{u})$  is the Gateaux (directional) derivative, defined by:

$$D_{\delta \mathbf{v}} f(\mathbf{u}) = \left\{ \frac{f}{d\alpha} (\mathbf{u} + \alpha \delta \mathbf{v}) \right\}_{\alpha=0}. \quad (9)$$

The first equation (7) defines the mechanical problem while the second one (8) defines the phase field problem. These two problems are coupled as shown in the following.

## 2.1 Mechanical problem

Eq. (7) can be developed as

$$\int_{\Omega} \frac{\partial \Psi}{\partial \boldsymbol{\varepsilon}}(\boldsymbol{\varepsilon}, d) : \boldsymbol{\varepsilon}(\delta \mathbf{u}) d\Omega - \int_{\partial \Omega_F} \mathbf{F}^* \cdot \delta \mathbf{u} d\Gamma = 0, \quad (10)$$

where

$$\frac{\partial \Psi}{\partial \boldsymbol{\varepsilon}}(\boldsymbol{\varepsilon}, d) = \boldsymbol{\sigma}. \quad (11)$$

For  $g(d) = (1-d)^2$  and with  $\Psi$  defined as in (3) we obtain:

$$\begin{aligned} \boldsymbol{\sigma} = & \left( (1-d)^2 + k \right) \left\{ \lambda \langle Tr \boldsymbol{\varepsilon} \rangle_+ \mathbf{1} + 2\mu \boldsymbol{\varepsilon}^+ \right\} \\ & + \lambda \langle Tr \boldsymbol{\varepsilon} \rangle_- \mathbf{1} + 2\mu \boldsymbol{\varepsilon}^-. \end{aligned} \quad (12)$$

where  $\mathbf{1}$  is the second-order identity tensor. It yields the classical weak form of the mechanical problem as:

$$\begin{aligned} \int_{\Omega} \boldsymbol{\sigma} : \boldsymbol{\varepsilon}(\delta \mathbf{u}) d\Omega &= \int_{\partial \Omega_F} \mathbf{F}^* \cdot \delta \mathbf{u} d\Gamma \\ \forall \delta \mathbf{u} \in H_0^1(\Omega). \end{aligned} \quad (13)$$

The Euler-Lagrange equation (strong form) associated with Eq. (13) is given by:

$$\nabla \cdot \boldsymbol{\sigma} = 0, \quad \boldsymbol{\sigma} \mathbf{n} = \mathbf{F}^* \text{ over } \partial \Omega_F, \quad \mathbf{u} = \mathbf{u}^* \text{ over } \partial \Omega_u. \quad (14)$$

## 2.2 Phase field problem

The first equation in (8) can be developed as:

$$\int_{\Omega} \frac{\partial \Psi}{\partial d} \delta d \, d\Omega + g_c \int_{\Omega} D_{\delta d} \gamma d\Omega = 0. \quad (15)$$

Choosing

$$\gamma = \frac{1}{2\ell} d^2 + \frac{\ell}{2} \nabla d \cdot \nabla d, \quad (16)$$

and for the quadratic form of the degradation function described above (note that a higher order  $\gamma(d)$  has been chosen in [?] to enhance the convergence), we obtain:

$$\begin{aligned} & \int_{\Omega} \left( 2\Psi^+ + \frac{g_c}{\ell} \right) d\delta d + g_c \ell \nabla d \cdot \nabla(\delta d) d\Omega \\ &= \int_{\Omega} 2\Psi^+ \delta d d\Omega. \end{aligned} \quad (17)$$

The choice of the numerical parameter  $\ell$  has been discussed e.g. in [? ? ? ?]. Enforcing the irreversibility condition  $\dot{d} \geq 0$  can be prescribed in several ways [? ?], e.g. by enforcing the Dirichlet condition  $d = 1$  at the nodes where the phase field has reached a value of  $d = 1$  or to enforce numerically  $d^{n+1} \geq d^n$  at each node. In this work, we adopt the formulation of Miehe [?] by introducing a history function  $\mathcal{H}$  which substitutes  $\tilde{\Psi}$  to handle loading and unloading and defined as:

$$\mathcal{H}(\mathbf{x}, t) = \max_{\tau \in [0, t]} \left\{ \tilde{\Psi}^+(\mathbf{x}, \tau) \right\}. \quad (18)$$

In that case, we obtain the weak form for the phase field problem as:

$$\begin{aligned} & \int_{\Omega} \left\{ \left( 2\mathcal{H} + \frac{g_c}{\ell} \right) d\delta d + g_c \ell \nabla d \cdot \nabla(\delta d) \right\} d\Omega \\ &= \int_{\Omega} 2\mathcal{H} \delta d \, d\Omega \quad \forall \delta d(\mathbf{x}) \in H_0^1(\Omega). \end{aligned} \quad (19)$$

Using the divergence theorem, the associated Euler-Lagrange equation to (17) is given by:

$$\left( 2\mathcal{H} + \frac{g_c}{\ell} \right) d - \ell g_c \Delta d = 2\mathcal{H} \quad (20)$$

with the boundary conditions

$$\nabla d \cdot \mathbf{n} = 0 \text{ over } \partial\Omega, \quad d = 1 \text{ over } \Gamma. \quad (21)$$

In (19),  $\Delta d$  denotes the Laplacian operator. It has been shown in [?] that this formulation is equivalent to applying the principle of maximum dissipation in a context of thermodynamics of irreversible phenomena.

### 3 Fracture models for the equivalent homogeneous medium

In the sequel, we seek to define models describing the fracture process for an equivalent homogeneous medium, where all details of heterogeneities are avoided (see figure 2).

The domain associated with the homogeneous solid is defined in an open domain  $\Omega \subset \mathbb{R}^D$ , where  $D$  denotes the space dimension. The corresponding boundary of  $\Omega$  is denoted by  $\partial\Omega$ , where  $\partial\Omega = \partial\Omega_u \cup \Omega_F$ ,  $\partial\Omega_u \cap \Omega_F = \emptyset$ , where traction forces  $\mathbf{F}^*$  are prescribed over the boundary  $\partial\Omega_F$  and displacements  $\mathbf{u}^*$  are prescribed over the boundary  $\partial\Omega_u$ . The quantities associated with the homogeneous medium are denoted by  $\overline{(\cdot)}$ , to distinguish them from their counterparts in the fully heterogeneous medium. Note that we assume that the scales are not separated, i.e. that the effective nonlinear properties at one point of the homogeneous structure cannot be obtained from the response of an RVE. Then, the approach we propose is to define models for the homogeneous medium based on the phase field method and to identify their characteristic parameters from specific fracture tests involving crack initiation and propagation in a fully heterogeneous medium. We will consider two cases: the first one when an isotropic phase field model for crack can be adopted, and the second one when an anisotropic model must be used to describe the crack propagation.

Under conditions on spatial distributions of heterogeneities, the effective elastic material can be found as isotropic, either under sufficient symmetry conditions within the microstructure [? ], or for random microstructures. However, these conditions do not necessarily lead to an isotropic damage description of the material, as the microcracks can be strongly oriented by the microstructure, the load history, or a nonlinear behavior of the phase, among others. In a context of regularized brittle fracture, the cracks have finite width and the ratio between this width and the characteristic size of the heterogeneities is another criterion leading or not to an effective anisotropic damage, as shown in the following examples.

#### 3.1 Isotropic effective fracture model

In this first case we consider an isotropic effective damage model for the homogeneous medium. Such model is usually not realistic in heterogeneous quasi brittle materials, as the load induces an orientation of the microcracks [? ]. However, we show in the following examples that in a context of regularized brittle fracture, this assumption can be acceptable for regular lattices when the characteristic length  $\ell$  in the phases of the heterogeneous medium is of the order of the dimensions of the heterogeneities or larger.

We remind that for quasi-brittle materials, it has been shown that the internal length  $\ell$  can be defined as a finite material parameter characterizing the medium, and that can be evaluated qualitatively from simple 1D considerations [? ? ? ], or identified quantitatively by inverse approach by combining simulations and experiments [? ? ]. For the above conditions of isotropic damage assumption of the homogeneous medium, we use the same model for the homogeneous model as the one in the heterogeneous medium, the only difference stemming from the values of the material parameters, which will be defined in the sequel. First, the equations of the mechanical problem for the homogeneous medium are given by:

$$\nabla \cdot \bar{\boldsymbol{\sigma}} = 0, \quad \bar{\boldsymbol{\sigma}} \mathbf{n} = \mathbf{F}^* \text{ over } \partial\Omega_F, \quad \bar{\mathbf{u}} = \mathbf{u}^* \text{ over } \partial\Omega_u, \quad (22)$$

with

$$\begin{aligned} \bar{\boldsymbol{\sigma}} = & \left( (1 - \bar{d})^2 + k \right) \left\{ \bar{\lambda} \langle Tr \bar{\boldsymbol{\varepsilon}} \rangle_+ \mathbf{1} + 2\bar{\mu} \bar{\boldsymbol{\varepsilon}}^+ \right\} \\ & + \bar{\lambda} \langle Tr \bar{\boldsymbol{\varepsilon}} \rangle_- \mathbf{1} + 2\bar{\mu} \bar{\boldsymbol{\varepsilon}}^-. \end{aligned} \quad (23)$$

The corresponding weak form is obtained as:

$$\begin{aligned} \int_{\Omega} \bar{\boldsymbol{\sigma}} : \bar{\boldsymbol{\varepsilon}}(\delta \bar{\mathbf{u}}) \, d\Omega &= \int_{\partial\Omega_F} \mathbf{F}^* \cdot \delta \bar{\mathbf{u}} \, d\Gamma \\ \forall \delta \bar{\mathbf{u}} \in H_0^1(\Omega). \end{aligned} \quad (24)$$

The equations of the phase field problem are given by:

$$\left( 2\bar{\mathcal{H}} + \frac{\bar{g}_c}{\bar{\ell}} \right) \bar{d} - \bar{\ell} \bar{g}_c \Delta \bar{d} = 2\bar{\mathcal{H}} \quad (25)$$

with the boundary conditions

$$\nabla \bar{d} \cdot \mathbf{n} = 0 \text{ over } \partial\Omega, \quad \bar{d} = 1 \text{ over } \bar{\Gamma}. \quad (26)$$

The corresponding weak form is given by:

$$\begin{aligned} \int_{\Omega} \left\{ \left( 2\bar{\mathcal{H}} + \frac{\bar{g}_c}{\bar{\ell}} \right) \delta \bar{d} + \bar{g}_c \bar{\ell} \nabla \bar{d} \cdot \nabla (\delta \bar{d}) \right\} \, d\Omega \\ = \int_{\Omega} 2\bar{\mathcal{H}} \delta \bar{d} \, d\Omega \quad \forall \delta \bar{d}(\mathbf{x}) \in H_0^1(\Omega). \end{aligned} \quad (27)$$

In the above,  $\bar{d}$  is the unknown fracture field for the homogeneous medium,  $\bar{\lambda}$  and  $\bar{\mu}$  are homogenized elastic parameters defined in section 3.3, and  $\bar{g}_c$  and  $\bar{\ell}$  are parameters to be identified (see section 3.4). In the above,  $\bar{\mathcal{H}}$  is a function similar to  $\mathcal{H}$  but using homogeneous quantities.

### 3.2 Anisotropic effective fracture model

When the microscopic characteristic length  $\ell$  is much lower than the size of the heterogeneities, the micro cracks strongly interact with the heterogeneities and this can induce preferential orientations of the cracks. In that case, an isotropic model for fracture is no longer valid to describe the crack propagation in the homogeneous medium. In such situation, even though the microstructure induces isotropic homogeneous elastic properties, the damage behavior can be fully anisotropic, as it is the case in regular lattices like honeycombs [?]. Then, we propose to employ the anisotropic phase field model proposed in [? ?], which is an extension to the model proposed in [?] to  $n$  preferential directions, to describe the fracture process in the homogeneous medium. Considering  $n$  preferential directions induced by the microstructure, which are assumed to be identified *a priori* from the microstructure knowledge, we define the total energy as

$$\begin{aligned}
E(\bar{\mathbf{u}}, \bar{d}_1, \bar{d}_2, \dots, \bar{d}_n) &= \int_{\Omega} \bar{\Psi}(\boldsymbol{\varepsilon}(\bar{\mathbf{u}}), \bar{d}_1, \bar{d}_2, \dots, \bar{d}_n) d\Omega \\
&+ \bar{g}_c \sum_{i=1}^n \int_{\Omega} \tilde{\gamma}_i(\bar{d}_i) d\Omega - \int_{\partial\Omega_F} \mathbf{F}^* \cdot \bar{\mathbf{u}} d\Gamma,
\end{aligned} \tag{28}$$

where  $\bar{d}_1, \bar{d}_2, \dots, \bar{d}_n$  are independent phase fields associated with each preferential direction  $i$ , and

$$\bar{\Psi}(\bar{\mathbf{u}}, \bar{d}_1, \bar{d}_2, \dots, \bar{d}_n) = \left( \prod_{i=1}^n g_i(\bar{d}_i) + k \right) \bar{\Psi}^+ + \bar{\Psi}^-, \tag{29}$$

where  $\bar{\Psi}^+$  and  $\bar{\Psi}^-$  are given by:

$$\bar{\Psi}^{\pm}(\boldsymbol{\varepsilon}) = \bar{\lambda} (\langle Tr(\bar{\boldsymbol{\varepsilon}}) \rangle_{\pm})^2 / 2 + \bar{\mu} Tr\{(\bar{\boldsymbol{\varepsilon}}^{\pm})^2\}, \tag{30}$$

and where  $\bar{\lambda}$  and  $\bar{\mu}$  are given by (43).

In Eq. (42),  $g_i(\bar{d}_i) = (1 - \bar{d}_i)^2$  is a degradation function associated with the damage variable  $\bar{d}_i$ . The crack density function  $\tilde{\gamma}_i(\bar{d}_i, \nabla \bar{d}_i, \boldsymbol{\omega}_i)$  associated to the  $i$ -th direction is defined as:

$$\tilde{\gamma}_i(\bar{d}_i, \nabla \bar{d}_i, \boldsymbol{\omega}_i) = \frac{1}{2\bar{\ell}} \bar{d}_i^2 + \frac{\bar{\ell}}{2} \boldsymbol{\omega}_i : \nabla \bar{d}_i \otimes \nabla \bar{d}_i, \tag{31}$$

where  $\boldsymbol{\omega}_i$  is a second-order orientation tensor defined by:

$$\boldsymbol{\omega}_i = \mathbf{1} + \bar{\beta}_i (\mathbf{1} - \mathbf{n}_i \otimes \mathbf{n}_i), \tag{32}$$

where  $\mathbf{n}_i$  is the unit normal vector to the preferential direction or plane of the damage. The anisotropic effect is parameterized by the coefficients  $\bar{\beta}_i$ . When  $\bar{\beta}_i = 0$  and  $n = 1$ , the isotropic phase field model is recovered. The new variational principle is written as a minimization with respect to  $\bar{\mathbf{u}}$  and the fields  $\bar{d}_i$ ,  $i = 1, 2, \dots, n$ :

$$\bar{\mathbf{u}}^{n+1}, \bar{d}_i^{n+1} = \underset{\substack{\bar{\mathbf{u}} \in \mathcal{K}_A \\ 0 \leq \bar{d}_i^n \leq \bar{d}_i^{n+1}}}{\text{Arg min}} E, \quad i = 1, 2, \dots, n. \tag{33}$$

In the sequel, we assume that the homogeneous material is elastically isotropic, but that the fracture process is anisotropic. This simplifies the definition of the model for separation into tensile and compressive parts in (4). Other type of splitting can be chosen (see [?] for isotropic elastic and [?] for anisotropic elastic case). The mechanical problem is then described by Eq. (22) with

$$\begin{aligned}
\bar{\boldsymbol{\sigma}} &= \left( \prod_{i=1}^n g_i(\bar{d}_i) + k \right) \left\{ \bar{\lambda} \langle Tr \bar{\boldsymbol{\varepsilon}} \rangle_+ \mathbf{1} + 2\bar{\mu} \bar{\boldsymbol{\varepsilon}}^+ \right\} \\
&+ \bar{\lambda} \langle Tr \bar{\boldsymbol{\varepsilon}} \rangle_- \mathbf{1} + 2\bar{\mu} \bar{\boldsymbol{\varepsilon}}^-.
\end{aligned} \tag{34}$$

The weak form remains unchanged as (24). The minimization process with respect to each  $\bar{d}_i$  field gives:

$$\int_{\Omega} \left\{ -2(1 - \bar{d}_i) \delta \bar{d}_i \prod_{i \neq j} g_j(\bar{d}_j) \bar{\Psi}^+ + \frac{\bar{g}_c}{\bar{\ell}} \bar{d}_i \delta \bar{d}_i + \bar{g}_c \bar{\ell} \nabla \bar{d}_i \boldsymbol{\omega}_i \nabla (\delta \bar{d}_i) \right\} d\Omega = 0, \quad i = 1, 2, \dots, n. \quad (35)$$

To ensure irreversibility of the fields  $\bar{d}_i$ , we use the history function defined in [?] as:

$$\hat{\mathcal{H}}_i = \max_{\tau \in [0, t]} \left\{ \prod_{i \neq j} g_j(d_j) \bar{\Psi}^+(\mathbf{x}, \tau) \right\}. \quad (36)$$

Replacing (36) into (35), the weak form for the  $i$ -th phase field problems is finally obtained as:

$$\int_{\Omega} \left\{ (2\hat{\mathcal{H}}_i + \frac{\bar{g}_c}{\bar{\ell}}) \bar{d}_i \delta \bar{d}_i + \bar{g}_c \bar{\ell} \nabla \bar{d}_i \boldsymbol{\omega}_i(\bar{\beta}_i) \nabla (\delta \bar{d}_i) \right\} d\Omega = \int_{\Omega} 2\hat{\mathcal{H}}_i \delta \bar{d}_i d\Omega \quad \forall \delta d(\mathbf{x}) \in H_1^0(\Omega). \quad (37)$$

For post-processing visualization purpose, an equivalent phase field  $d_{eq}$  can be calculated from  $\bar{d}_i$  ( $i = 1, 2, \dots, n$ ) such that:

$$(1 - d_{eq})^2 = \prod_{i=1}^n g_i(\bar{d}_i)^2. \quad (38)$$

In this model, in addition to the effective elastic parameters  $\bar{\lambda}$  and  $\bar{\mu}$ , the following fracture parameters have to be identified:  $\bar{g}_c$ ,  $\bar{\ell}$ ,  $\bar{\beta}_i$ ,  $i = 1, 2, \dots, n$ . For the sake of simplification, we assume that  $\bar{\beta}_1 = \bar{\beta}_2 = \dots = \bar{\beta}_n = \bar{\beta}$ . Then, three material parameters need to be identified instead of two for the homogeneous model. It is worth noting that in (32), the different preferential orientations  $\mathbf{n}_i$  have to be identified. In the present work, we consider simple microstructures where these orientations can be assumed a priori based on simple geometric considerations (see e.g. Fig. 23).

### 3.3 Computation of effective elastic parameters

The effective elastic parameters are computed by means of classical computational homogenization. Let  $\Omega^{RVE}$  be the domain associated with an RVE of the microstructure (see e.g. Fig. 4) and  $\partial\Omega^{RVE}$  its boundary. The problem (14) is solved with  $d = 0$ ,  $\mathbf{F}^* = \mathbf{0}$  and boundary conditions

$$\mathbf{u}^*(\mathbf{x}) = \bar{\boldsymbol{\varepsilon}} \mathbf{x} + \tilde{\mathbf{u}}(\mathbf{x}) \quad \text{over } \partial\Omega, \quad (39)$$

where  $\tilde{\mathbf{u}}(\mathbf{x})$  is a periodic function over  $\Omega$ . Eq. (39) corresponds to prescribing a constant overall strain  $\bar{\boldsymbol{\varepsilon}}$  over the RVE. The effective elastic tensor is deduced from

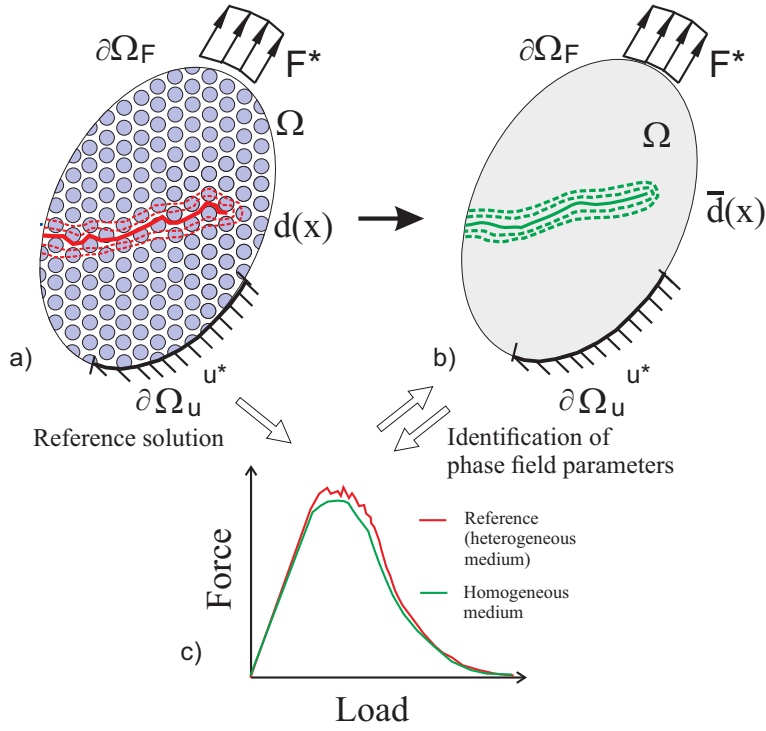


**Fig. 2:** Identification procedure for constructing the equivalent homogeneous medium.

$$\bar{\mathbb{C}} = \langle \mathbb{A}(\mathbf{x}) : \mathbb{C}(\mathbf{x}) \rangle \quad (40)$$

where  $\langle \cdot \rangle$  is the averaging operator over  $\Omega^{RVE}$ , and

$$A_{ijkl}(\mathbf{x}) = \varepsilon_{ij}^{(kl)}(\mathbf{x}) \quad (41)$$

is the fourth-order localization tensor,  $\varepsilon_{ij}^{(kl)}(\mathbf{x})$  is the strain field in the RVE for an applied overall strain

$$\bar{\varepsilon}^{(kl)} = \frac{1}{2} (\mathbf{e}_k \otimes \mathbf{e}_l + \mathbf{e}_l \otimes \mathbf{e}_k) \quad (42)$$

where  $\mathbf{e}_i$  are unit basis vectors. For 2D plane strain isotropic material, the effective coefficients are deduced from (40) by

$$\bar{\lambda} = \bar{C}_{1122}, \quad \bar{\mu} = \bar{C}_{1212} = \frac{\bar{C}_{1111} - \bar{C}_{1122}}{2}. \quad (43)$$

### 3.4 Effective fracture parameters

To determine the unknown fracture parameters related to the homogeneous medium, an inverse approach employing numerical simulations over the heterogeneous medium

as a reference for the identification of the parameters is proposed. In the case of the isotropic fracture model, the unknown parameters are  $\bar{g}_c$  and  $\bar{\ell}$ , while in the anisotropic model the unknown parameters are  $\bar{g}_c$ ,  $\bar{\ell}$  and  $\bar{\beta}$ . A schematic of the overall identification procedure is provided in Fig. 2. First, a fracture simulation is performed on a structure whose heterogeneities are explicitly described and fully meshed. We recall that we assume a non-separation of scales, i.e. that the characteristic size of the heterogeneities is not too small as compared to the characteristic dimensions of the structure. A force-displacement-curve is obtained, which is used as data for the identification. Then, the same problem is solved for the homogeneous model, and the unknown fracture parameters are adapted until a tolerance criterion is reached. In the present work, we have used the following functional:

$$J = \int_0^{u_{max}^*} \left( F^{hom}o(u^*) - F^{ref}(u^*) \right)^2 du^*; \quad (44)$$

with  $u_{max}^*$  is the maximum applied displacement in the simulation involving the full heterogeneous structure,  $F^{hom}o$  is the force response of the homogeneous structure, and  $F^{ref}$  is the reference response of the heterogeneous structure.

The problem to identify the unknown parameters is then given by

$$\{\bar{g}_c, \bar{\ell}, \bar{\beta}\} = \text{Arg min } J. \quad (45)$$

It is worth noting that in the present work, we did not introduced in the optimization problem an objective related to the error in the direction of the crack. This point should be investigated in future studies. To ensure a right reproduction of main crack directions, we have then constrained the values of  $\bar{\beta}$  to sufficiently large ranges. A numerical illustration of the effects of  $\bar{\beta}$  with respect to the damage anisotropy is provided in Appendix 8.

As the problem (45) is non quadratic and may involve many local minima, efficient optimization algorithms must be employ. In the present work, we have used the simplex search algorithm described in [? ], while many other strategies are possible from the vast literature on optimization algorithms.

## 4 Numerical examples

In this section, the procedure described in sections 3.3, 3.4 to construct the homogeneous damage model is applied to several practical examples, including hard particles-matrix composites and porous media with regular lattices. For all the examples, linear 3-node elements have been used for the different meshes.

### 4.1 Periodic composite with hard inclusions

#### 4.1.1 Test for identification of macroscopic parameters

We consider the heterogeneous structure depicted in Fig. 3, composed of a matrix and circular inclusions which are distributed over a periodic hexagonal lattice (see Fig. 4). The radius of inclusions is  $r = 0.025$  mm and the distance  $h$  between the centers of the inclusions is equal to 0.08 mm. The material parameters of the

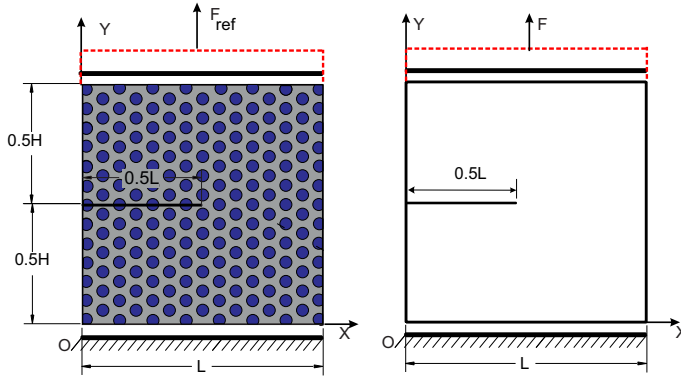


**Fig. 3:** Test (T1) used to identify the parameters of the homogeneous crack propagation model: heterogeneous media (left) and homogeneous media (right).

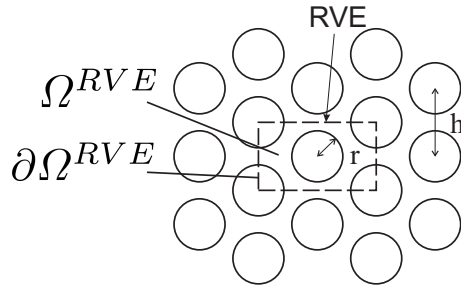


**Fig. 4:** Periodic hexagonal lattice of circular inclusions or pores.

matrix are:  $\mu_1 = 121.15$  MPa,  $\lambda_1 = 80.77$  MPa,  $g_c^1 = 0.0027$  kN/mm, where  $\mu_1$ ,  $\lambda_1$  and  $g_c^1$  denote the matrix Lamé's parameters and Griffith-type critical energy release rate associated with the matrix, respectively. The material parameters for the inclusions are chosen as twice those of the matrix:  $\mu_2 = 2\mu_1$ ,  $\lambda_2 = 2\lambda_1$  MPa,  $g_c^2 = 2g_c^1$ . To analyze the influence of the microstructural damage parameters on the identified homogeneous model, different crack width values are considered:  $\ell = \{r/5, 2r/5, r, 2r\}$ . The corresponding meshes for the heterogeneous structure (see Fig. 3, left) contain:  $3.4 \times 10^5$ ,  $8.8 \times 10^4$ ,  $8.8 \times 10^4$  and  $2.2 \times 10^4$  elements respectively. The corresponding meshes for the homogeneous structure (see Fig. 3, left) contain  $3.2 \times 10^5$ ,  $8.0 \times 10^4$ ,  $8.0 \times 10^4$  and  $2.0 \times 10^4$  elements respectively. We note that both discretizations for heterogeneous and homogeneous structures contain similar number of elements. This has been chosen for validation purpose. However, once identified, the homogeneous model can be used within a context of adaptive mesh refinement, to drastically reduce computational times as compared to directly solve the heterogeneous structure problem.

In each case, we first identify the macroscopic damage parameters  $\bar{g}_c$  and  $\bar{\ell}$  and validate the model through several tests implying crack initiation and propagation for other configurations. The test used to identify the parameters is described in Fig. 3. The size of the samples is  $L \times H = 1 \times 1$  mm<sup>2</sup>. In the following tests, dimensions  $L$  and  $H$  will remain unchanged.

case	$\bar{\ell}$ ,	$\bar{g}_c$
$\ell = 5 \times 10^{-3}$	$4.950 \times 10^{-3}$	$3.797 \times 10^{-3}$
$\ell = 1 \times 10^{-2}$	$1.012 \times 10^{-2}$	$3.700 \times 10^{-3}$
$\ell = 2.5 \times 10^{-2}$	$2.525 \times 10^{-2}$	$3.595 \times 10^{-3}$
$\ell = 5 \times 10^{-2}$	$5.000 \times 10^{-2}$	$3.491 \times 10^{-3}$

**Table 1:** Identified parameters for the equivalent homogeneous media corresponding to the hard inclusions composite:  $\bar{g}_c, \bar{\ell}$  obtained for different regularized lengths  $\ell$  in the microscopic phases.

In this first case, we assume that  $\ell$  is of the order of the radius  $r$  of the inclusions. We recall that  $\ell$  is here regarded as a material parameter for the matrix. It has been shown experimentally and numerically in [?] that when this parameter is larger than the heterogeneities in the medium, then the crack path is not much affected by these heterogeneities, and an isotropic damage model can accurately reproduce the crack propagation. However as expected, the equivalent medium involves both elastic and damage parameters which take different values than in the matrix. Then, under these assumption (the case when  $\ell \ll r$  will be treated in section 4.3), we use the same phase field model for the homogeneous model, but identify the unknown parameters  $\bar{\ell}$  and  $\bar{g}_c$  by the procedure described in section 3.4.

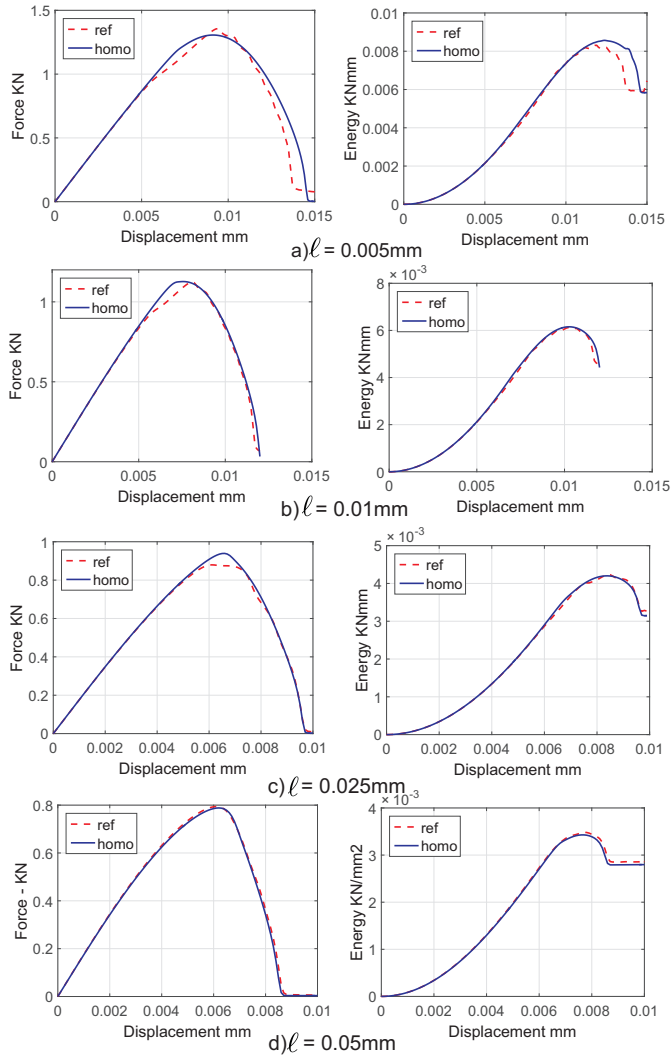
In that case, the isotropic damage model described in section 3.1 is used for the homogeneous model. The first step is to compute the effective elastic parameters of the homogeneous domain from the RVE described in Fig. 4. The results give  $\bar{\mu} = 101.66$  MPa and  $\bar{\lambda} = 149.70$  MPa. In a second step, we identify the parameters of the macroscopic phase field model using the tension test described in Fig. 3, called (T1). The sample includes an initial horizontal crack of length  $0.5L$  at  $y = 0.5H$ . Displacements are fixed along  $x$ - and  $y$ - direction on the lower end ( $y = 0$ ). On the upper end ( $y = H$ ), the displacements are fixed along  $x$ -direction and prescribed along the  $y$ -direction through  $u_y = \bar{u}$ . Incremental displacement steps  $\Delta u = 10^{-4}$  mm are prescribed until complete failure of the specimen.

A force-displacement curve is obtained for the heterogeneous medium (see Fig. 3) and used as a reference solution for the identification. The same test is conducted on the homogeneous medium to fit the unknown effective coefficients  $\bar{g}_c$  and  $\bar{\ell}$ .

In the following examples, we use as an initial guess for the optimization procedure the following values:  $\bar{\ell}^0 = \ell$  and  $\bar{g}_c^0 = f_1 g_c^1 + f_2 g_c^2$ , where  $f_1$  and  $f_2$  are the respective volume fractions of each phase.

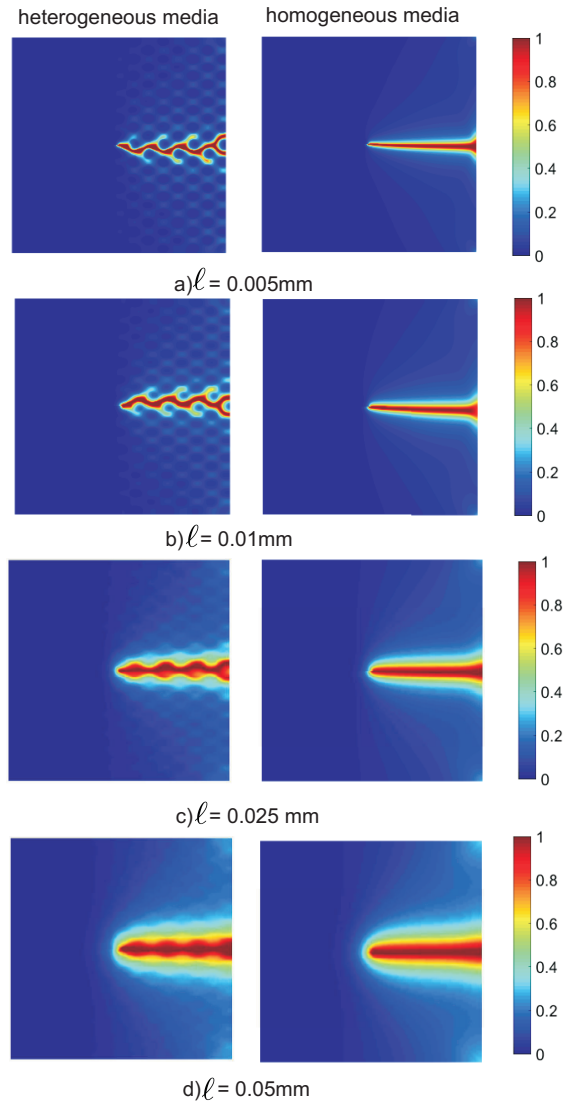
Table 1 shows the resulting effective parameters ( $\bar{g}_c, \bar{\ell}$ ) in four cases, corresponding to different crack widths at the microscale:  $\ell = \{r/5, 2r/5, r, 2r\}$ . We can note that the optimized values of  $\bar{\ell}$  do not vary significantly as compared to  $\ell$  which is expected as the crack path is not much affected by the presence of the inclusions in that case. However, we can note that  $\bar{g}_c$  takes different values as compared to the matrix and that the lower the microscopic crack width  $\ell$  is, the larger the macroscopic toughness.

Fig. 5 compares the force-displacement responses and their corresponding energy-displacement curves using the identified parameters for different values of micro crack widths  $\ell$ . The crack paths are compared in Fig. 6. We can note that the larger  $\ell$ , the better agreement between micro and effective response or crack pat-



**Fig. 5:** Comparison between reference solution, "ref" (heterogeneous medium) and equivalent homogeneous medium, "homo": (a) Force - displacement curve and (b) Energy- displacement curve for the traction test (T1).

terns is found. Even though the homogeneous model is not able to capture all branching and secondary microcracks as in the microscopic model, the main direction and length of the crack is well captured with the homogeneous model. With smaller  $\ell$ , the microscopic heterogeneous model induces more fluctuations, and then the macroscopic model only captures the averaged trends, which is expected.



**Fig. 6:** Crack networks for the traction test (T1): comparison between the reference solution (heterogeneous medium) and the equivalent homogeneous medium.

#### 4.1.2 Validation tests

In this section, the identified homogeneous model is validated on other configurations than the one used to identify the effective parameters. The first validation test (called V1) uses the same cracked sample as described above, but the loading induces shear. The second validation test (V2) involves a doubly cracked specimen. Both tests are described in Fig. 7. For the shear test, the geometry of the sample is the same as in the traction test. The displacements are blocked along

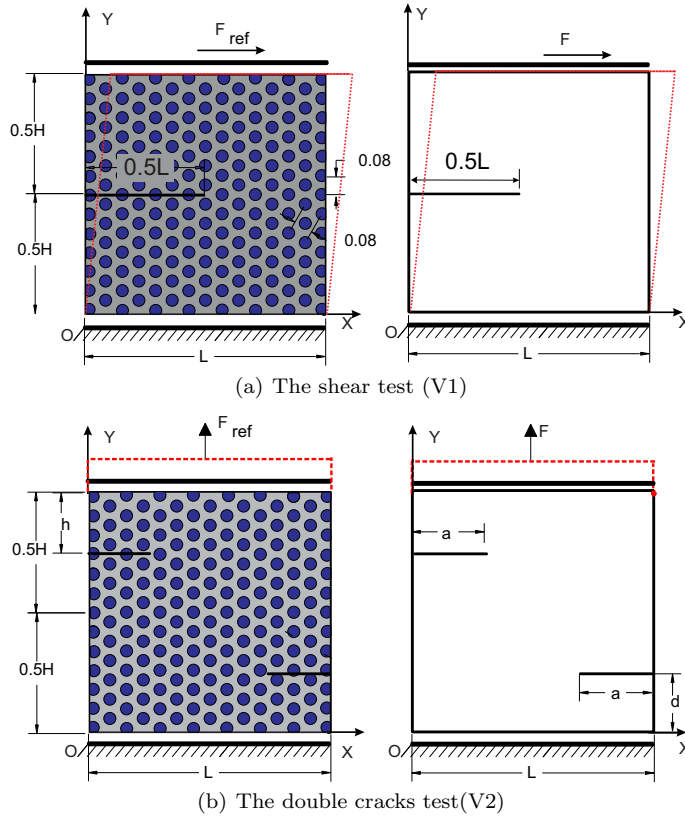


**Fig. 7:** Validation tests of periodic composite structure with hard inclusions: a shear test (V1) and a double crack test (V2).

both direction on the lower end. On the upper end, the displacements are fixed along the  $y$ -direction and are prescribed along the  $x$ -direction with displacement increments  $\Delta u_x = 5 \times 10^{-5}$  mm. In the double cracks test depicted in Fig. 7(b), the rectangular domain contains two initial cracks whose lengths are  $a = 0.25$  mm and their position is defined by  $d = 0.25$  mm. The displacements are blocked along both direction on the lower end. On the upper end, the displacements are fixed along the  $x$ -direction and are prescribed along the  $y$ -direction with displacement increments  $\Delta u_y = 1 \times 10^{-4}$  mm.

Results are presented in Figs (8-11). Here again, a good agreement is found between the reference model and the homogeneous one. When the microscopic crack width  $\ell$  is small as compared to the heterogeneities, the homogeneous model no more captures the local fluctuations of both response and microcrack networks, but the overall trends are well captured.

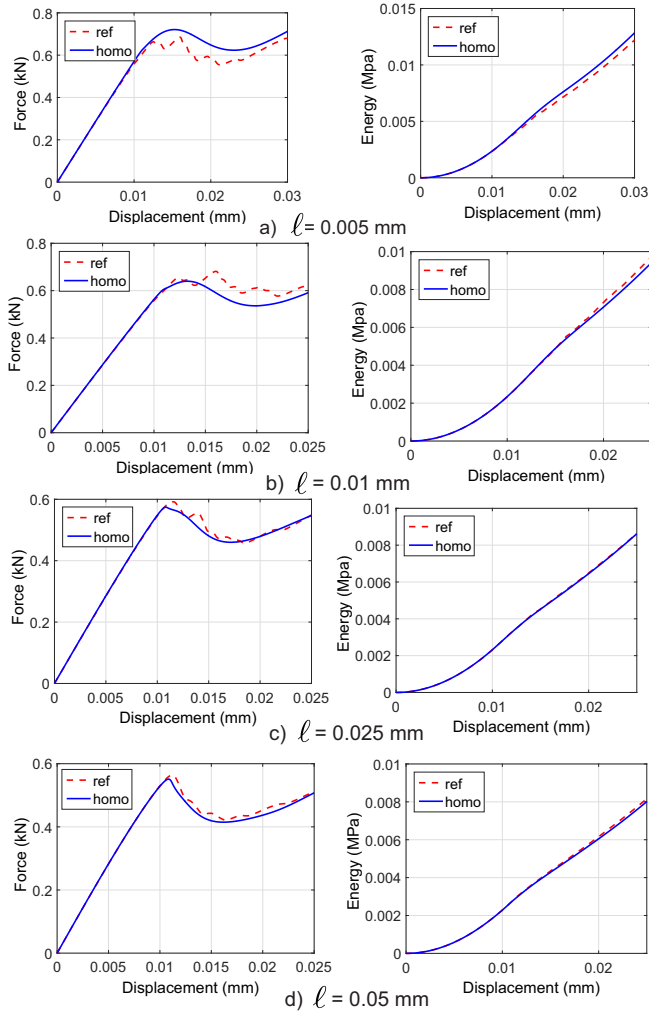


**Fig. 8:** Comparison between the response of the homogeneous medium ("homo") and the heterogeneous medium ("ref") using equivalent parameters in the Table 1: Force - displacement (first column) and Energy- displacement (second column) in the validation shear test (V1).

#### 4.2 Periodic quasi-brittle porous lattice structure: isotropic macroscopic fracture model

In this section, we consider a porous lattice structure with periodic distribution of pores on a hexagonal lattice (see Fig. 4). The material properties of the skeleton are  $\mu = 121.15$  MPa,  $\lambda = 80.77$  MPa,  $g_c = 0.0027$  kN/mm and the crack width is  $\ell = 0.025$  mm. To evaluate the influence of the ratio  $\ell/r$ , we consider two sizes of pores while maintaining the same value for  $\ell$  and using:  $r = 0.02$  mm,  $h = 0.064$  mm and  $r = 0.01$  mm,  $h = 0.032$  mm. The test used to identify the macroscopic parameters of the phase field model is the same as in the previous example (Fig.

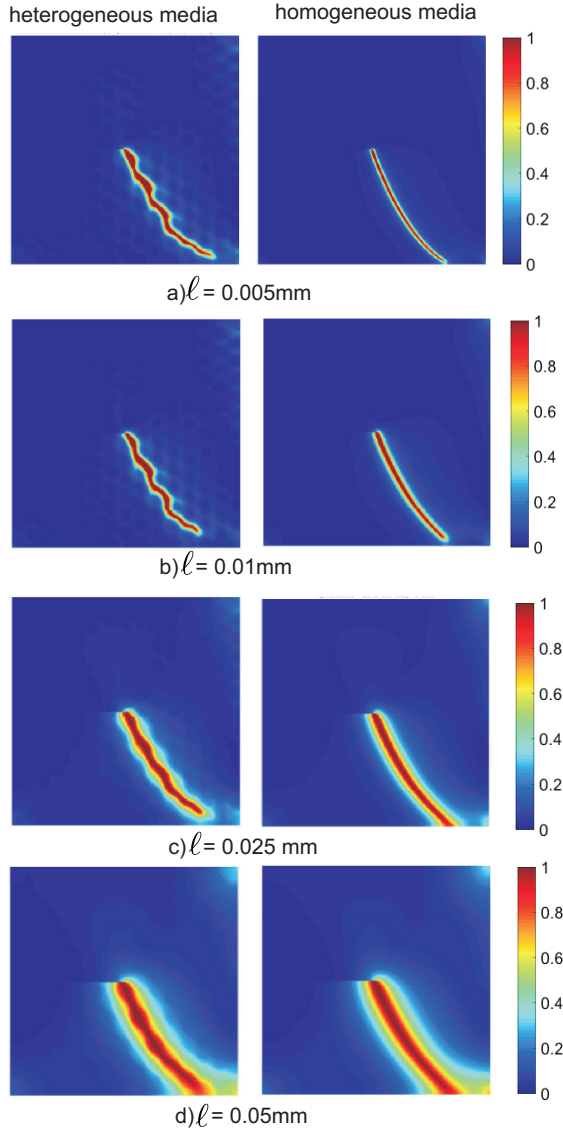


**Fig. 9:** Comparison of phase field distribution of the heterogeneous medium and the homogeneous medium in shear test (V1) for various regularized lengths.

3, Test (T1)), except that the heterogeneities are here voids. We will show that in the case where  $\ell$  is of the same order than  $r$ , an isotropic phase field can provide a good approximation for the response of the heterogeneous model, but with some restrictions. The case when  $\ell$  is much lower than the radius of the pores will be treated in section 4.3. It is worth noting that here again, the elastic effective medium is isotropic.

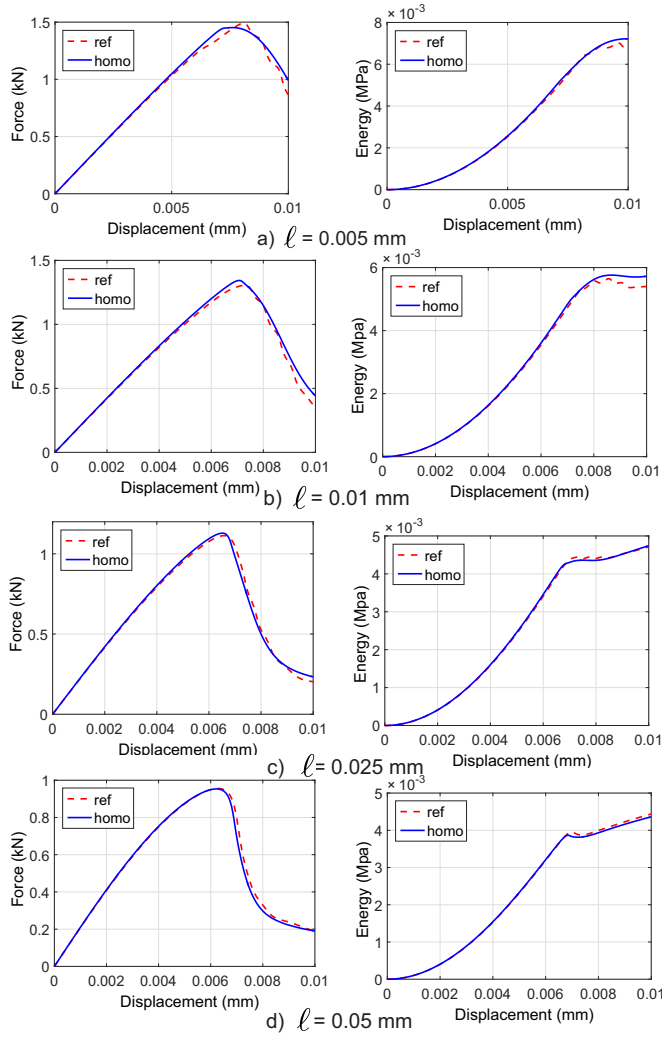


**Fig. 10:** Comparison of F-u curves and E-u curves of the heterogeneous medium ("ref") and homogeneous medium ("homo") in the double cracks test (V2) for various regularized lengths.

We first consider the case  $\ell/r = 2.5$ , corresponding to a porosity of 0.345. In this case, the effective elastic parameters for the RVE depicted in Fig. 4 are obtained as  $\bar{\mu} = 35.96$  MPa;  $\bar{\lambda} = 42.86$  MPa and the identified parameters for the effective phase field model are obtained as:  $\ell = 0.025$  mm and  $\bar{g}_c = 0.0017624$  kN/mm. In that case, the mesh of the heterogeneous structure contains  $1.5 \times 10^4$  elements and the mesh of the homogeneous structure contains  $2 \times 10^4$  elements.

In a second case,  $\ell/r = 1.25$ ,  $r = 0.02$  mm and  $h = 0.064$  mm (see Fig. 4), which induces a porosity of 0.33. The effective elastic parameters are in this case obtained as:  $\bar{\mu} = 32.06$  MPa,  $\bar{\lambda} = 40.10$  MPa. The identified damage parameters for the homogeneous model are obtained as:  $\bar{g}_c = 0.001827$  KN/mm;  $\bar{\ell} = 0.0250$

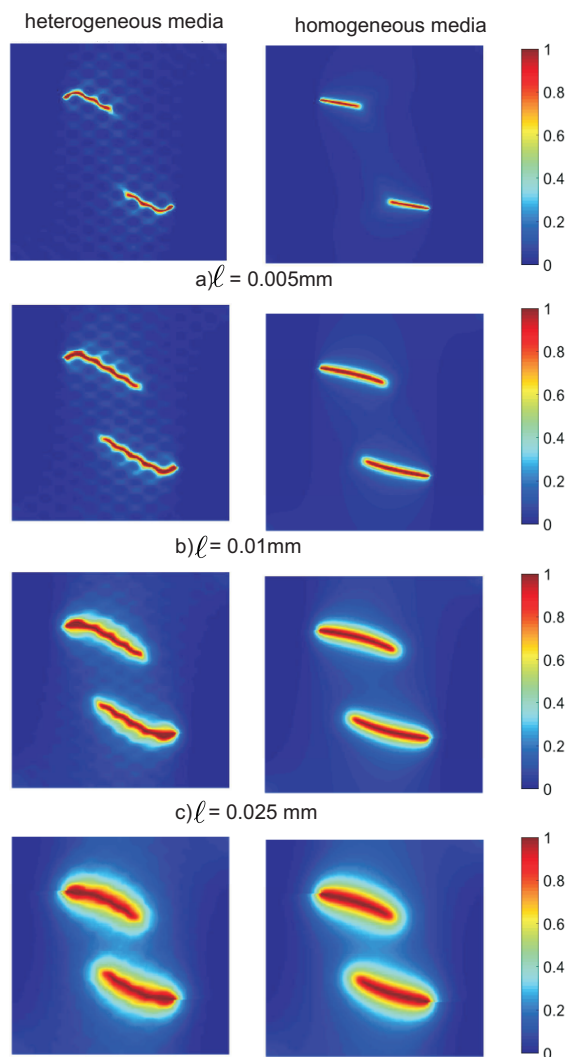


**Fig. 11:** Comparison of F-u curves and E-u curves of the heterogeneous medium and homogeneous medium in the double cracks test (V2) with various regularized length.

mm. Here, the mesh of the heterogeneous structure contains  $6.1 \times 10^4$  elements and the mesh of the homogeneous structure contains  $8 \times 10^4$  elements.

Two validation tests, called V1 and V2, have been performed in both case. The validation test V1 involves a shear load as described in Fig. 7 (a) while the test V2 implies a sample with two initial cracks as described in Fig. 7 (b). The conditions and geometries are identical as in the previous examples. The results are presented in Fig. 12 and 14.

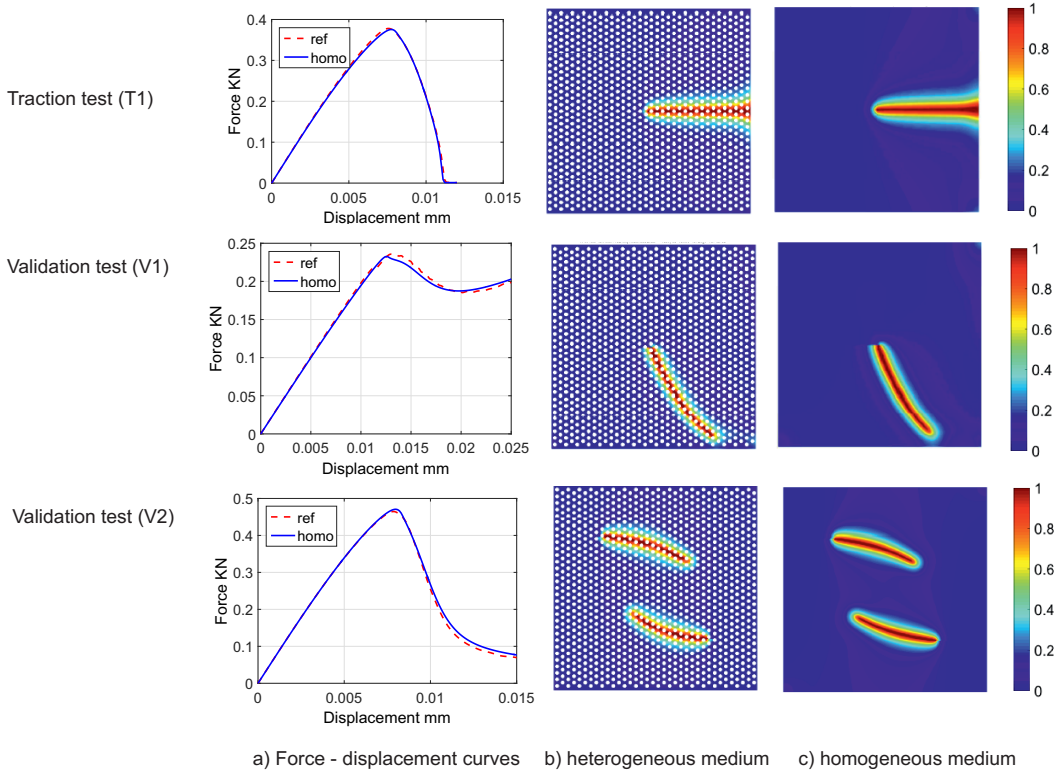


**Fig. 12:** Porous media with  $\ell/r = 2.5$ : comparison of  $F$ - $u$  relations and crack profiles in three tests: T1,V1,V2

In the case  $\ell/r = 2.5$ , we can observe from both tests V1 and V2 (see Figs. 12 and 14), that the force-displacement curve as well as the crack path are accurately reproduced by the homogeneous model. In Fig. 13(a) and Fig. 13(b), the energy - displacement  $E - \bar{u}$  and surface energy - displacement  $E_s - \bar{u}$  are plotted for both models, showing a good agreement.

Results for the porous medium with  $\ell/r = 1.25$  are provided in Fig. 14. We can note that in this case, even though the force-displacement curve is in good agreement with the reference model, the crack path tends to deviate. This shows the limit of the isotropic model for the homogeneous medium in the case  $\ell < r$ . To circumvent this issue, the anisotropic phase field model described in section 3.2 is adopted in the next section, to treat the case  $\ell \ll r$ .

#### 4.3 Periodic porous lattice: anisotropic macroscopic fracture model

In this example, we assume that the internal length  $\ell$  is much smaller than the size of the pores. In this case, the isotropic model for fracture propagation described in section 3.1 can no longer describe some preferential crack paths induced by the microstructure. Then, the anisotropic phase field framework described in section

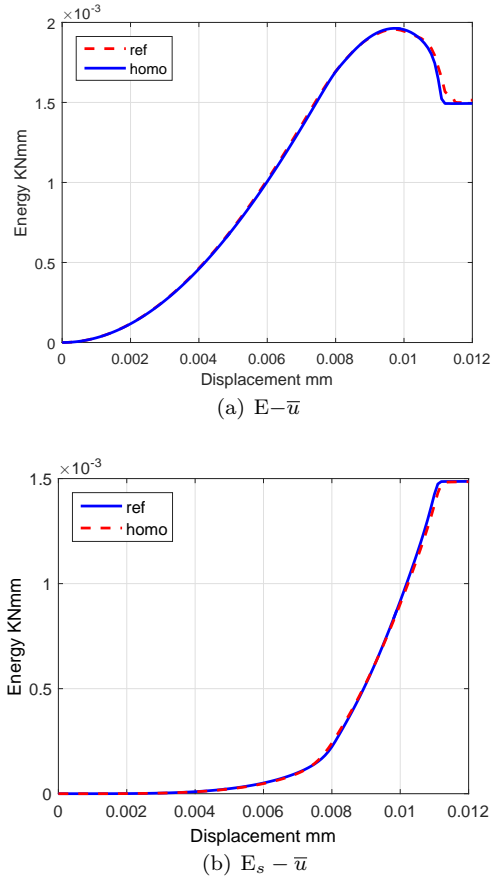


**Fig. 13:** Comparison between (a) the total energy and (b) the crack surface energy  $E_s$  for the heterogeneous medium "ref" and the homogeneous medium "homo".

3.2 is adopted. The porous media with parameters  $r = 0.02$  mm and  $h = 0.064$  mm (see Fig. 4) is employed. Here,  $\ell = 0.0025$  mm, which corresponds to  $\ell = r/8$ . In that context, there are three damage parameters to be identified, in addition to the effective elastic parameters:  $\bar{\ell}$ ,  $\bar{g}_c$ , and the parameter related to anisotropy  $\bar{\beta}$  in Eq. (54). Note that regarding elastic properties, the media remains isotropic, and can be characterized by the two effective Lamé's parameters  $\bar{\lambda}$  and  $\bar{\mu}$ . These two effective parameters have the same values as in the previous example. In the studied lattice of Fig. 4, there are three obvious main preferential directions for crack propagation, corresponding to  $n = 3$  in Eq. (37).

The above phase field parameters are identified using the traction test described in Fig. 3, where 175 load increments  $\Delta u_Y = 1.5 \times 10^{-4}$  mm are prescribed in the first 50 steps and  $\Delta u_Y = 1 \times 10^{-4}$  mm during the following steps. A comparison between the homogeneous model and the reference heterogeneous one are depicted in Fig. 15, showing that the homogeneous model is able to capture the preferential direction for the crack path induced by the microstructure. The initial guess of

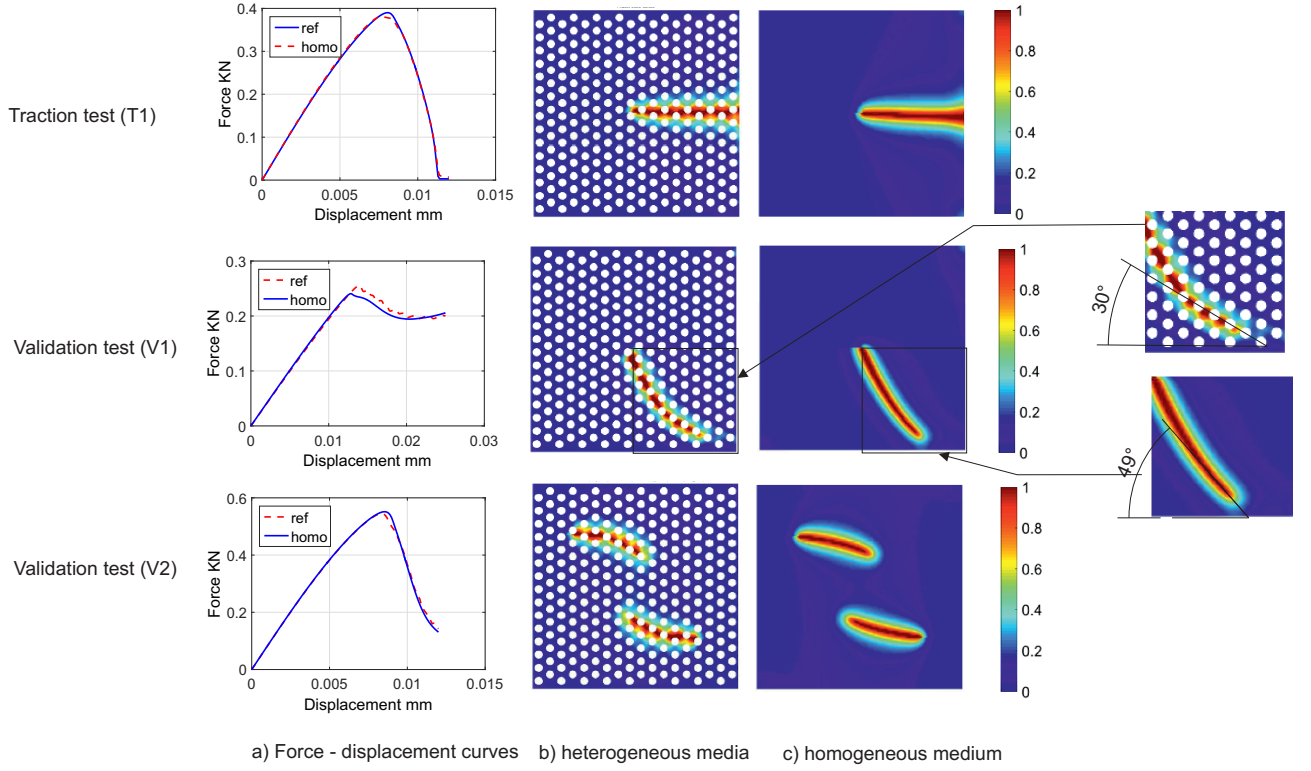


**Fig. 14:** Porous media with  $\ell/r = 1.25$ : comparison of  $F$ - $u$  relations and crack profiles in the three tests T1, V1 and V2.

$\bar{\beta}$  for the optimization procedure is taken as  $\bar{\beta}^0 = 50$ . The following macroscopic parameters are obtained through the optimization procedure:  $\bar{g}_c = 2.388 \times 10^{-3}$  kN/mm,  $\bar{\ell} = 0.0082$  mm and  $\bar{\beta} = 50.002$ .

#### 4.3.1 Validation tests

In this section, we validate the anisotropic model on different configurations. The first set of tests consists in cracked samples as described in Figs. 16.

The first one, described in Fig. 16 (a), involves the same geometry than used for identification of the model, but a more complex loading involving both traction and shear on the upper end of the structure. On the lower end, displacements are fixed in both directions while prescribed in both directions with increments  $\Delta u_Y = \Delta u_X = 1 \times 10^{-4}$  on the upper end. Comparison between the reference solution (heterogeneous medium) and the homogeneous one is provided in Fig. 17. Remarkably, both force response and crack paths are well described by the homogeneous model. We can even note that the set of microcracks which develops on the upper-right-end are captured by the homogeneous model.

Next, a traction test is considered, where the crack is shorter than in the test used for identification, as described in Fig.16 (b). The boundary conditions are

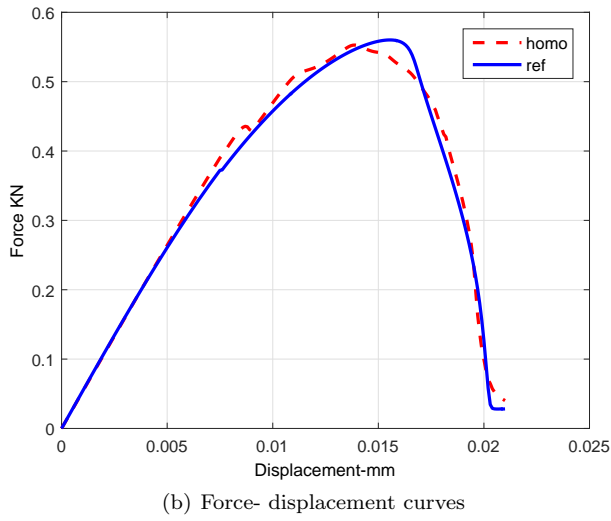
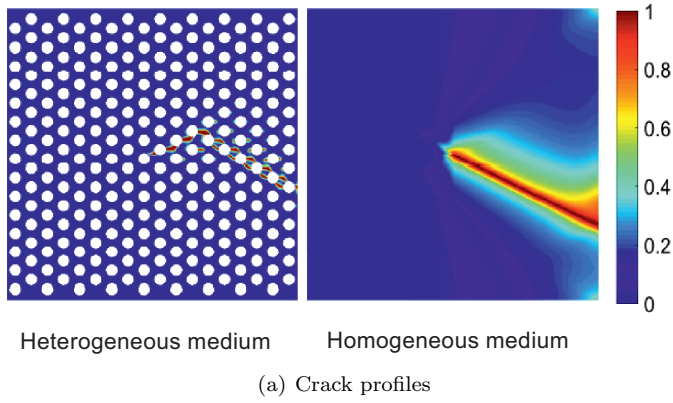


**Fig. 15:** Comparison of heterogeneous media (M1) and homogeneous media (M2) in the identification test. In M1,  $F_{max} = 0.55$  kN at  $\bar{u} = 0.01390$ mm and in M2,  $F_{max} = 0.5601$ kN at  $\bar{u} = 0.0156$ mm.

the same as in the identification test. The crack length is equal to  $0.1 L$ . Results are presented in Figs. 18. We can note from Fig. 18 (a) that the main direction of the crack is well captured. Here, even though the global shape of the response is similar, we note in Fig. 18 (b) some discrepancies between both solution for Force-displacement curves: in the heterogeneous medium  $F_{max} = 1.23$  kN at  $u = 0.0166$  mm while in homogeneous media  $F_{max} = 1.04$  kN at  $u = 0.0178$  mm. The error in the maximum force is about 15 %.

A third test implies a porous lattice structure containing two cracks as depicted in Fig. 16(c). Displacements are fixed in both direction on the lower end ( $y = 0$ ) and prescribed along the  $y$ - direction with 300 displacement increments  $\Delta u_Y = 1 \times 10^{-4}$  mm. Results are presented in Fig.19. We can observe from 19(a) that

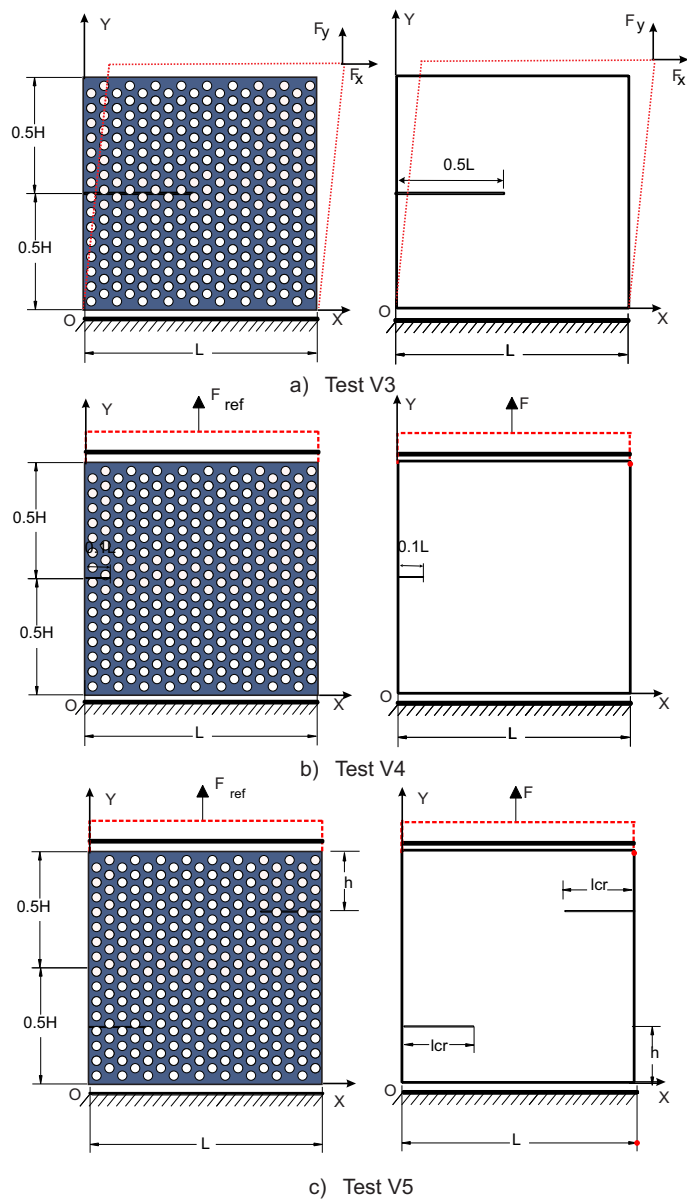


**Fig. 16:** Validation tests V3, V4 and V5 for the homogeneous anisotropic fracture model: porous plates with initial cracks.

the crack path are accurately captured by the homogeneous model and the second preferential direction is activated, this cannot be achieved by using one preferential direction. However, we note from Fig. 19 (b) that even though the maximum force is well captured, the failure of the sample occurs later in the homogeneous model. This issue might be corrected in future studies by modifications of the degradation

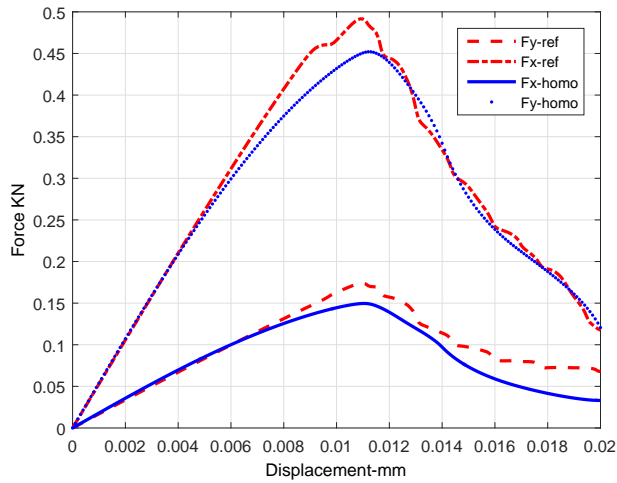
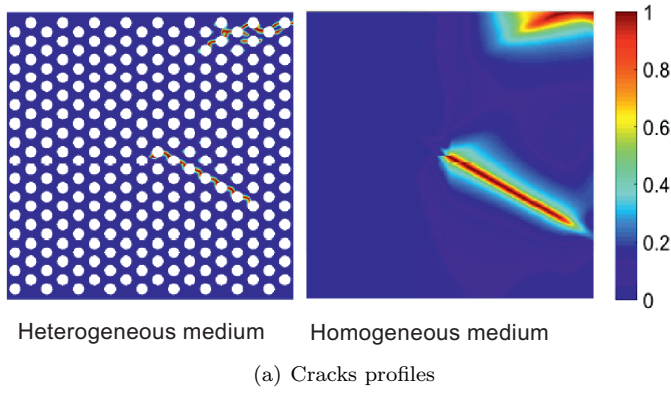


**Fig. 17:** Comparison between the heterogeneous media (M1) and homogeneous media (M2) in the complex test:  $Fx_{max} = 0.1737\text{KN}$  at  $\bar{u} = 0.0109\text{mm}$ ,  $Fy_{max} = 0.4916\text{ kN}$  at  $\bar{u} = 0.0110\text{mm}$  in M1 and  $Fx_{max} = 0.1496$  at  $\bar{u} = 0.0111\text{ mm}$ ,  $Fy_{max} = 0.4520\text{ kN}$  at  $\bar{u} = 0.0113\text{ mm}$  in M2.

function  $g(d)$  and by formulations implying a threshold (see e.g. [? ]). Note that these formulations imply more parameters, which should then be also identified in the present framework. Another source of discrepancy comes from the fact that the crack propagation is strongly influenced by the environment of the onset of the crack, which can be complex in the heterogeneous medium. Then, room for improvement of the method is possible.

In these examples,  $8.8 \times 10^5$  elements have been used for the mesh of the heterogeneous structure, and  $1.25 \times 10^5$  elements have been used for the mesh of the homogeneous structure.

Finally, a lattice structure with periodic pores is considered, which contains a large hole in its center, as depicted in Fig. 20. The dimensions of the sample are  $L \times H = 2 \times 1.2\text{ mm}^2$ . Displacements are fixed in both directions on the lower face

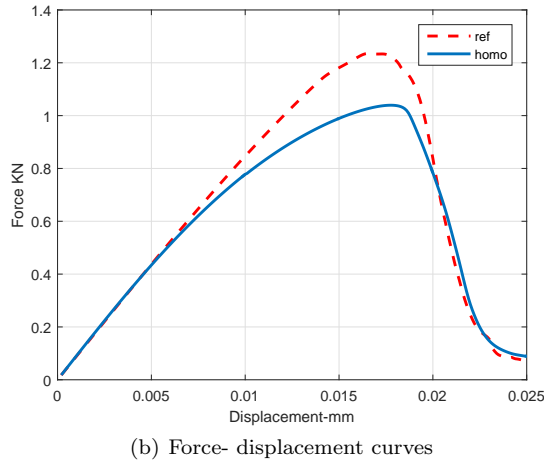
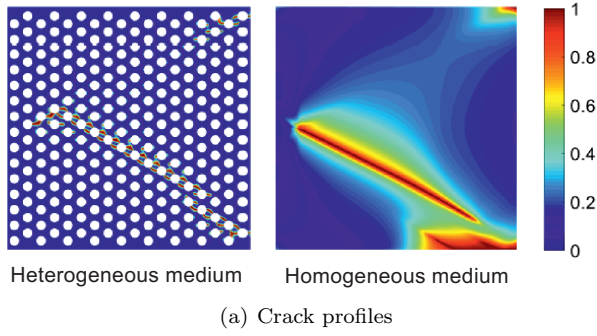


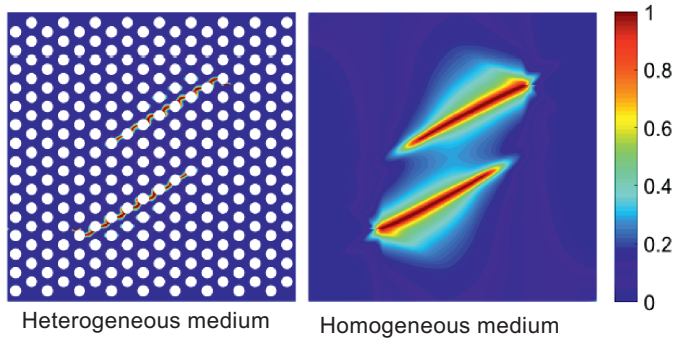
**Fig. 18:** Traction test with shorter crack: in heterogeneous media  $F_{max} = 1.2353\text{KN}$  at  $\bar{u} = 0.0166$  mm while in homogeneous media  $F_{max} = 1.0393$  kN at  $\bar{u} = 0.0178$  mm.

( $y = 0$ ) and only  $y$ -displacements are prescribed on the upper face  $y = H$  during 200 displacement increments  $\Delta u_Y = 1.5 \times 10^{-4}$ . Here,  $1.03 \times 10^6$  elements have been used for the mesh of the heterogeneous structure, and  $3.88 \times 10^5$  elements have been used for the mesh of the homogeneous structure.

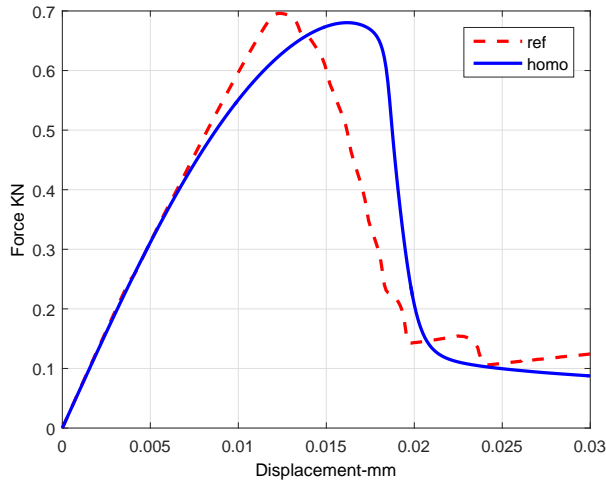
Comparisons between the full-field (micro) model and the homogeneous model are presented in Figs. 21 and 22). We can note a good agreement between both models, both regarding the evaluation of the traction response and on the crack paths whose overall directions are accurately captured.

## 5 Conclusion

A procedure was proposed to construct an equivalent homogeneous model for heterogeneous lattices submitted to crack propagation in the case of non-separated scales. Unlike the case of separated scales where an RVE can be considered for the micro scale, for non-separated scales, i.e. when the characteristic dimensions of inclusions are much smaller than the dimensions of the structure, the notion



(a) Crack profiles of two media



(b) Force- displacement curves

**Fig. 19:** Comparison of heterogeneous media(M1) and homogeneous media (M2) in the double crack test:  $F = 0.6959\text{KN}$  at  $\bar{u} = 0.0124\text{mm}$  in M1; and  $F = 0.6803\text{KN}$  at  $u = 0.0164\text{mm}$  in M2

of RVE does not exist anymore. In the present work, we have proposed to use at the scale of the homogeneous medium phase field models, whose parameters are identified through numerical crack propagation tests in fully heterogeneous samples. Two main cases have been considered: when the microscale crack width is comparable with the dimensions of the heterogeneities, and when the crack width is much smaller. For the first case, we have shown that an isotropic phase field model accurately captures both mechanical response of the sample as well as overall crack paths. In the second case, the microstructure interacts much more with the cracks, inducing preferential directions in regular lattices, and requiring an anisotropic phase field. The results show that the homogeneous model is able to reproduce both force response and crack paths also in this situation. The identified models for crack propagation in heterogeneous media have then been validated through

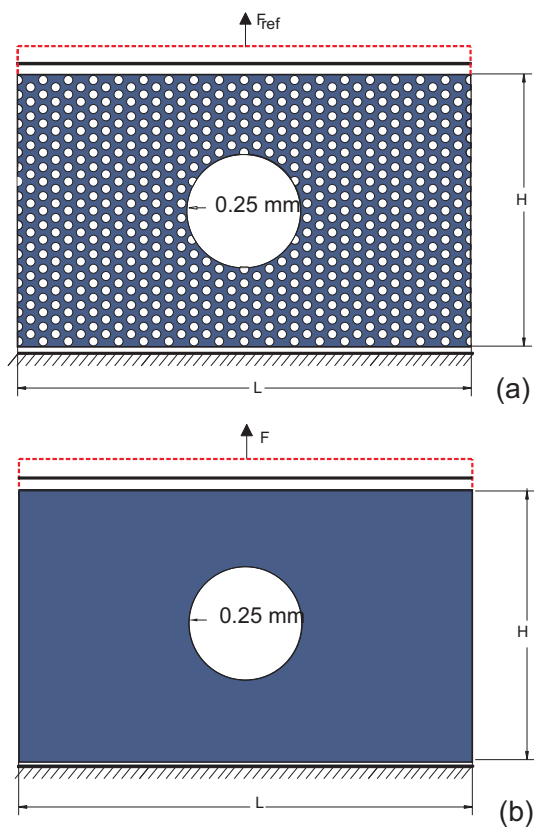


**Fig. 20:** Validation test V6: a plate with a center hole.

numerical tests involving different configurations, showing the applicability of the method. The identified model can then be used for crack propagation simulations without the need for meshing implicitly all heterogeneities.

## 6 Acknowledgement

The financial support of Institut Universitaire de France (IUF) for J.Y. is gratefully acknowledged and National Foundation for Science and Technology Development (NAFOSTED) for N.N.

## 7 Appendix: FEM discretization of phase field problems

### 7.1 Isotropic phase field model

A classical Finite Element discretization of the phase field problem weak form (27) yields at loading increment  $n + 1$ :

$$\mathbf{K}_{\bar{d}} \bar{\mathbf{d}} = \mathbf{F}_d, \quad (46)$$

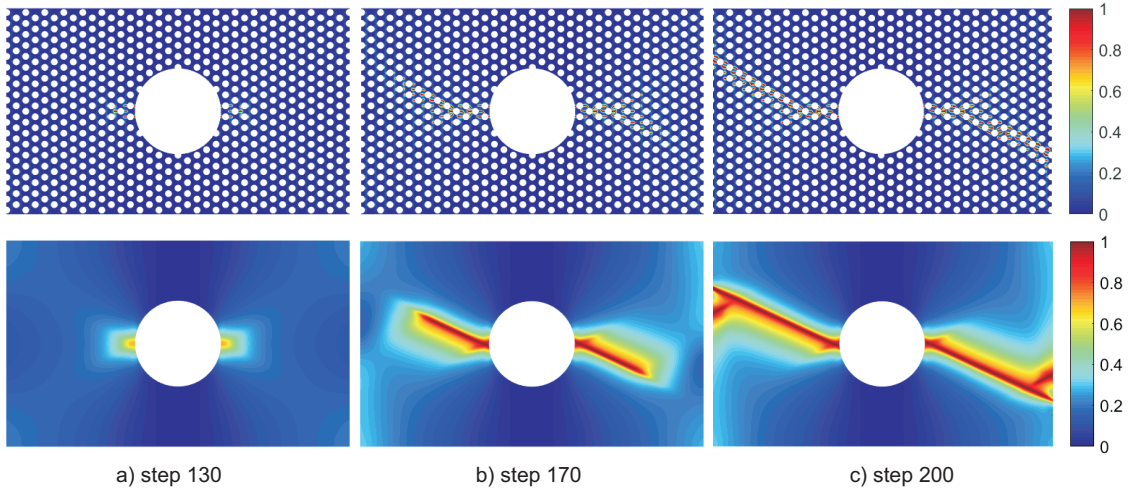


**Fig. 21:** Comparison between heterogeneous and homogeneous models: crack patterns for (a)  $u^* = 0.0195$  mm; (b)  $u^* = 0.0255$  mm, (c)  $u^* = 0.030$  mm.

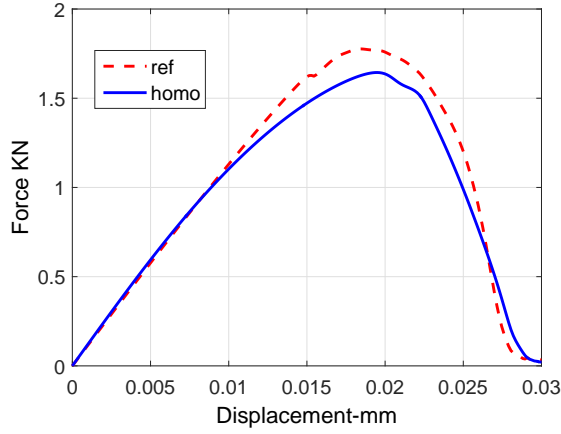


**Fig. 22:** Test V6 (plate with a center hole): comparison between the heterogeneous medium response ("ref") and the homogeneous solution ("homo").

where

$$\begin{cases} \mathbf{K}_d = \int_{\Omega} \left\{ (2\bar{\mathcal{H}} + \frac{\bar{g}_c}{\bar{\ell}}) \mathbf{N}_d^T \mathbf{N}_d + \bar{g}_c \bar{\ell} \mathbf{B}_d^T \mathbf{B}_d \right\} d\Omega, \\ \mathbf{F}_d = \int_{\Omega} 2\mathbf{N}_d^T \bar{\mathcal{H}} d\Omega. \end{cases} \quad (47)$$

In (54), the crack driving force  $\bar{\mathcal{H}}$  is computed by Eq. (18),  $\mathbf{N}_d$  is the matrix of shape functions associated with damage variable  $d$  and  $\mathbf{B}_d$  is the derivative matrix of  $\mathbf{N}_d$ . For the sake of simplicity, we use the approximation proposed in [?] within

a staggered scheme:

$$\boldsymbol{\varepsilon}_{n+1}^+ \simeq \mathbb{P}_n^+ : \boldsymbol{\varepsilon}_{n+1}, \quad \boldsymbol{\varepsilon}_{n+1}^- \simeq \mathbb{P}_n^- : \boldsymbol{\varepsilon}_{n+1}, \quad (48)$$

and

$$\langle \text{tr} \boldsymbol{\varepsilon}_{n+1} \rangle_{\pm} \simeq \mathcal{R}^{\pm}(\boldsymbol{\varepsilon}_n) \text{tr} \boldsymbol{\varepsilon}_{n+1}, \quad (49)$$

$$\mathcal{R}^{\pm}(\boldsymbol{\varepsilon}_n) = (\text{sign}(\pm \text{tr} \boldsymbol{\varepsilon}_n) + 1)/2. \quad (50)$$

For more details about strain tensor split, see [? ?]. The matrix form for the displacement problem is written as:

$$\{\mathbf{K}_1(\bar{\mathbf{d}}_{n+1}, \mathbf{u}_n) + \mathbf{K}_2(\mathbf{u}_n)\} \bar{\mathbf{u}}_{n+1} = \mathbf{F}_{n+1} \quad (51)$$

where

$$\begin{cases} \mathbf{K}_1(\bar{\mathbf{d}}, \mathbf{u}_n) = (g(\bar{d}) + k) \int_{\Omega} \mathbf{B}^T (\mathbf{C}_{\bar{\lambda}} \mathcal{R}^- + \mathbf{C}_{\bar{\mu}} \mathbf{P}^+) \mathbf{B} \, d\Omega; \\ \mathbf{K}_2(\mathbf{u}_n) = \int_{\Omega} \mathbf{B}^T (\mathbf{C}_{\bar{\lambda}} \mathcal{R}^- + \mathbf{C}_{\bar{\mu}} \mathbf{P}^-) \mathbf{B} \, d\Omega, \\ \mathbf{F} = \int_{\partial\Omega_F} \mathbf{N}^T \bar{\mathbf{F}} \, d\Gamma. \end{cases} \quad (52)$$

Setting the vector forms of strains and stress as:  $\boldsymbol{\varepsilon} = [\boldsymbol{\varepsilon}_{11}; \boldsymbol{\varepsilon}_{22}; \sqrt{2}\boldsymbol{\varepsilon}_{12}]$  and  $\boldsymbol{\sigma} = [\boldsymbol{\sigma}_{11}; \boldsymbol{\sigma}_{22}; \sqrt{2}\boldsymbol{\sigma}_{12}]$ ,  $\mathbf{C}_{\bar{\lambda}} = [\bar{\lambda} \ \bar{\lambda} \ 0; \bar{\lambda} \ \bar{\lambda} \ 0; 0 \ 0 \ 0]$  and  $\mathbf{C}_{\bar{\mu}} = 2[\bar{\mu} \ \bar{\mu} \ \bar{\mu}; \bar{\mu} \ \bar{\mu} \ \bar{\mu}; \bar{\mu} \ \bar{\mu} \ \bar{\mu}]$  in 52.

The discretization of the microscopic phase field problem (19) is identical to the above one.

## 7.2 Anisotropic phase field model

The matrix form associated to the weak form (35) to solve phase fields  $d_{i(i=1,2..n)}$  at load increment  $n + 1$  is given by:

$$\mathbf{K}_{d_i} \bar{\mathbf{d}}_i = \mathbf{F}_{d_i}, \quad (53)$$

where :

$$\begin{cases} \mathbf{K}_{d_i} = \int_{\Omega} \left\{ (2\bar{\mathcal{H}}_i + \frac{\bar{g}_c}{\ell}) \mathbf{N}_d^T \mathbf{N}_d + \bar{g}_c \bar{\ell} \mathbf{B}_d^T \omega_i(\bar{\beta}) \mathbf{B}_d \right\} \, d\Omega, \\ \mathbf{F}_{d_i} = \int_{\Omega} 2\mathbf{N}_d^T \bar{\mathcal{H}}_i \, d\Omega. \end{cases} \quad (54)$$

The discretization of the elastic problem is the same as in (51) except that a new degradation function is employed, as:

$$\mathbf{K}_1(\mathbf{d}_{i(n+1)}, \mathbf{u}_n) = \left( \prod_{i=1}^n g_i(\bar{d}_i) + k \right) \int_{\Omega} \mathbf{B}^T (\mathbf{C}_{\bar{\lambda}} \mathcal{R}^- + \mathbf{C}_{\bar{\mu}} \mathbf{P}^+) \mathbf{B} \, d\Omega; \quad (55)$$

### 8 Appendix: Anisotropic effects in anisotropic phase field model in the case $n = 3$

in this section, we analyze the damage anisotropic effects with respect to the parameter  $\bar{\beta}$ . For this purpose, we consider a circular domain with regular lattice of pores ( $R = 0.32$  mm) with a center hole of radius ( $r = 0.03$  mm), see Fig. 23 (b). The critical energy release rate is chosen as  $g_c = 1N/mm^2$ . The dimension is depicted in Fig.23b. The heterogeneous medium will be replaced by a homogeneous media with 3 preferential directions. The normal vectors for this lattice are  $\mathbf{n}_1 = [-1/2; \sqrt{3}/2]$ ;  $\mathbf{n}_2 = [-1; 0]$ ;  $\mathbf{n}_3 = [-1/2; -\sqrt{3}/2]$ . We prescribe  $d_i (i = 1, 2, 3) = 1$  around the inner hole and solve the phase field problem for zero displacements. We consider the average surface energy  $G_s(\theta)$  ( $N/mm^2$ ) in different direction around the center. Here, the average  $G_s(\theta)$  is computed according to:

$$G_s(\theta) = \frac{1}{r_2 - r_1} g_c \int_{r_1}^{r_2} \gamma(d) dr \quad (56)$$

where  $r_1 = r$  and  $r_2 = r_1 + 0.1$  mm as shown in Fig. 23 (c). We can note from Fig.24 that the convexity of the polar plot, which gives information about weakest directions for crack propagation, depends on both  $\beta$  and  $\ell$ .

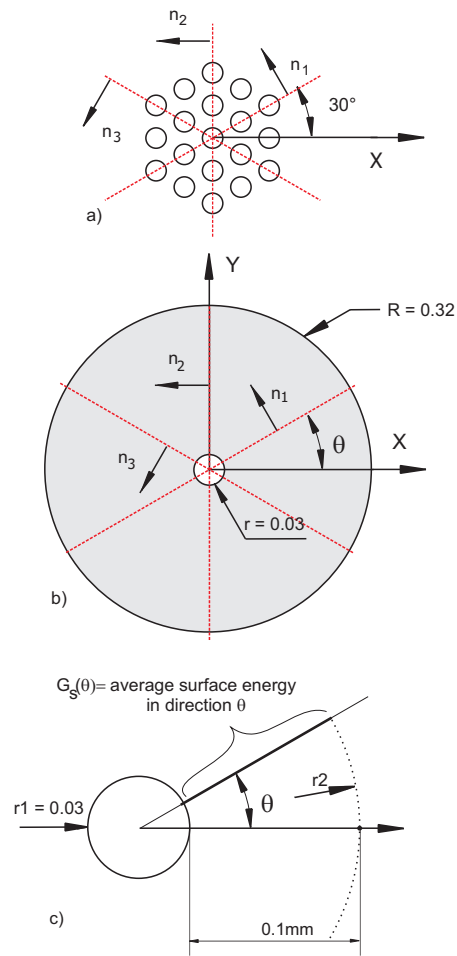


**Fig. 23:** The 3 main directions for preferential crack propagation in the hexagonal lattice: (a); main normal directions  $\mathbf{n}_1, \mathbf{n}_2, \mathbf{n}_3$  (b) circular domain; (c) distances for computing the crack surface energy.

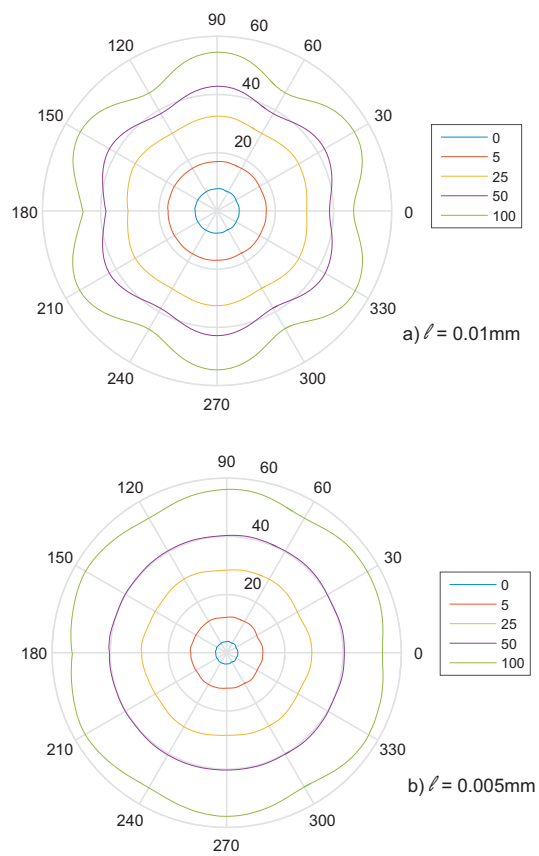


**Fig. 24:** Polar plots of  $G_s(\theta)$  with respect to  $\beta$ : (a) when  $\bar{\beta} = 50$ , the convexity is clear in case  $\ell = 0.01$ , while the material behaves as a isotropic one for the case  $\ell = 0.005$ .